Mitochondrial Dysfunction and Lipid Accumulation in the Human Diaphragm during Mechanical Ventilation

Martin Picard[1,2,3*‡], Boris Jung[1,4,5*], Feng Liang[1*], Ilan Azuelos[1], Sabah Hussain[1,6], Peter Goldberg[1,6], Richard Godin[7], Gawiyou Danialou[1], Rakesh Chaturvedi[6], Karolina Rygiel[8], Stefan Matecki[5], Samir Jaber[4,5], Christine Des Rosiers[9], George Karpati[10], Lorenzo Ferri[11], Yan Burelle[7], Douglass M. Turnbull[8], Tanja Taivassalo[2,3,10], and Basil J. Petrof[1]

[1]Meakins-Christie Laboratories, [2]Department of Kinesiology and Physical Education, [3]Respiratory Epidemiology and Clinical Research Unit, and [10]Montreal Neurological Institute, McGill University, Montreal, Quebec, Canada; [4]Anesthesiology and Critical Care Department, Saint Eloi Hospital, and [5]Institut National de la Santé et de la Recherche Médicale U-1046, Arnaud de Villeneuve Hospital, Centre Hospitalier Universitaire, Montpellier, France; [6]Critical Care and Respiratory Divisions and [11]Department of Thoracic Surgery, McGill University Health Centre and Research Institute, Montreal, Quebec, Canada; [7]Faculty of Pharmacy and [9]Montreal Heart Institute, Université de Montréal, Montreal, Quebec, Canada; and [8]Mitochondrial Research Group, Centre for Brain Ageing and Vitality, Newcastle University, Newcastle, United Kingdom

Rationale: **Mechanical ventilation (MV) is associated with adverse effects on the diaphragm, but the cellular basis for this phenomenon, referred to as ventilator-induced diaphragmatic dysfunction (VIDD), is poorly understood.**

Objectives: **To determine whether mitochondrial function and cellular energy status are disrupted in human diaphragms after MV, and the role of mitochondria-derived oxidative stress in the development of VIDD.**

Methods: **Diaphragm and biceps specimens obtained from brain-dead organ donors who underwent MV (15–176 h) and age-matched control subjects were compared regarding mitochondrial enzymatic function, mitochondrial DNA integrity, lipid content, and metabolic gene and protein expression. In addition, diaphragmatic force and oxidative stress after exposure to MV for 6 hours were evaluated in mice under different conditions.**

Measurements and Main Results: **In human MV diaphragms, mitochondrial biogenesis and content were down-regulated, with a more specific defect of respiratory chain cytochrome-*c* oxidase. Laser capture microdissection of cytochrome-*c* oxidase–deficient fibers revealed mitochondrial DNA deletions, consistent with damage from oxidative stress. Diaphragmatic lipid accumulation and responses of master cellular metabolic sensors (AMP-activated protein kinase and sirtuins) were consistent with energy substrate excess as a possible stimulus for these changes. In mice, induction of hyperlipidemia worsened diaphragmatic oxidative stress during MV, whereas transgenic overexpression of a mitochondria-localized antioxidant (peroxiredoxin-3) was protective against VIDD.**

Conclusions: **Our data suggest that mitochondrial dysfunction lies at the nexus between oxidative stress and the impaired diaphragmatic contractility that develops during MV. Energy substrate oversupply relative to demand, resulting from diaphragmatic inactivity during MV, could play an important role in this process.**

AT A GLANCE COMMENTARY

Scientific Knowledge on the Subject

Mechanical ventilation (MV) is associated with diaphragmatic dysfunction in humans and animal models, but little is known about the underlying cellular triggers and molecular mechanisms.

What This Study Adds to the Field

This study shows that mitochondrial function is severely disrupted in human MV diaphragms, with impaired mitochondrial biogenesis and enzymatic activities, and mitochondrial DNA damage. Furthermore, a transgenic mouse model points to mitochondria-derived oxidative stress as a likely trigger of ventilator-induced diaphragmatic dysfunction. Finally, metabolic substrate oversupply in MV diaphragms is identified as a potential instigator of mitochondrial dysfunction and oxidative stress under these conditions, thus suggesting new therapeutic avenues in patients with diaphragmatic dysfunction and weaning failure.

(*Received in original form June 1, 2012; accepted in final form September 6, 2012*)

* These authors contributed equally to this work.

‡ Current address: Center for Mitochondrial and Epigenomic Medicine, Children's Hospital of Philadelphia and University of Pennsylvania, Philadelphia, PA.

Supported by grants from the McGill University Health Centre Research Institute (B.J.P., P.G.); Canadian Institutes of Health Research (B.J.P., T.T., S.H., C.D.R., Y.B., M.P.); Natural Sciences and Engineering Research Council of Canada (T.T., S.H., Y.B., M.P.); Fonds de Recherche en Santé du Québec (T.T., Y.B., McGill University Health Centre members); INSERM (S.M., S.J.); Societé Française d'Anesthésie Réanimation and Association Pour l'Assistance et la Réhabilitation à Domicile (B.J.); and the Newcastle University Centre for Brain Ageing and Vitality (D.M.T.).

Author Contributions: B.J.P. and T.T. supervised the study. All authors participated in the study design. P.G., G.D., R.C., S.M., S.J., G.K., and L.F. were involved in surgical procurement of muscle specimens from patients. M.P. designed and performed the histologic, biochemical, electron microscopy, and molecular genetics experiments with assistance from R.G. and K.R.; analyzed the data; prepared the figures; and wrote the manuscript with B.J.P. and T.T. B.J. and I.A. conducted the animal experiments. F.L. performed the gene expression experiments. Y.B. provided experimental reagents. B.J.P., M.P., B.J., I.A., F.L., T.T., S.H., C.D.R., D.M.T., and R.G. were involved in data analysis and preparation of the manuscript.

Correspondence and requests for reprints should be addressed to Basil J. Petrof, M.D., Meakins-Christie Laboratories, 3626 Saint Urbain Street, Montreal, PQ, H2X 2P2 Canada. E-mail: basil.petrof@mcgill.ca

This article has an online supplement, which is accessible from this issue's table of contents at www.atsjournals.org

Am J Respir Crit Care Med Vol 186, Iss. 11, pp 1140–1149, Dec 1, 2012
Copyright © 2012 by the American Thoracic Society
Originally Published in Press as DOI: 10.1164/rccm.201206-0982OC on September 28, 2012
Internet address: www.atsjournals.org

Keywords: ventilator-induced diaphragmatic dysfunction; oxidative stress; mitochondrial DNA; metabolic oversupply; diaphragmatic fatigue

Mechanical ventilation (MV) is one of the most frequently used interventions in the intensive care unit. Respiratory muscle dysfunction is often an important factor in the inability to successfully wean patients from MV (1–3), leading to an increase in medical complications and healthcare costs (4). Respiratory muscle weakness in this setting is likely related in part to the fact that MV itself causes diaphragmatic muscle fiber atrophy and injury in animals and humans (5–7), a condition termed ventilator-induced diaphragmatic dysfunction (VIDD) (8). The diaphragm, in contrast to other skeletal muscles, is normally activated rhythmically on a 24-hour basis. MV imposes a unique

form of muscle disuse on the diaphragm, because the latter is simultaneously mechanically unloaded, intermittently shortened, and electrically suppressed by the ventilator breaths (9). Under these conditions, the energetic requirements of the diaphragm muscle fibers are also greatly reduced.

A large body of evidence points to oxidative stress as an essential element in the development of VIDD (10–14), but the primary source of increased reactive oxygen species (ROS) generation in the diaphragms of patients undergoing MV remains unclear (9). In addition, the underlying driving mechanisms that initiate and sustain excessive ROS production from diaphragmatic muscle fibers during MV are poorly understood. It is known that when energy substrate supplies substantially exceed cellular demands, this can trigger increased ROS production from mitochondria (15–17), a mechanism that has been implicated in the pathogenesis of metabolic syndrome and type 2 diabetes (18–21). In this regard, excessive mitochondrial superoxide production is a common feature of several metabolic oversupply models (20), and can damage mitochondrial DNA (mtDNA) (22, 23) and induce insulin resistance as a protective mechanism to mitigate this process (24). Cellular sensing of energetic oversupply also leads to a down-regulation of mitochondrial biogenesis (25), which further compromises mitochondrial function. Whether or not such a situation exists in the diaphragm during MV has not been studied. However, a decrease in mitochondrial function resulting from MV would be especially ill-suited to the situation faced by the diaphragm during attempts at weaning from the ventilator, when the energetic demands placed on the muscle are suddenly and substantially increased.

In the present study, we hypothesized that MV could trigger two major deleterious effects on diaphragmatic mitochondrial function. First, the reduced energy requirements of the diaphragm during MV might be "appropriately" interpreted as a signal to down-regulate mitochondrial biogenesis and enzymatic function. Second, a state of relative energetic oversupply versus demand induced by the lack of diaphragmatic activity during MV could exist, which favors increased mitochondrial ROS production (15–17). This could have damaging effects on the mitochondrial genome and other cellular components. All of these changes would be anticipated to increase the susceptibility of the diaphragm to muscle weakness and fatigue, thereby contributing to weaning failure.

To test our hypothesis, we studied the diaphragms of brain-dead organ donor patients who received MV in the intensive care unit before organ harvest, and compared these specimens with control diaphragmatic biopsies obtained during thoracic surgery for removal of solitary lung nodules. In addition, proof-of-concept experiments to evaluate the roles of metabolic oversupply and mitochondria-derived oxidative stress in the pathogenesis of VIDD were performed in mechanically ventilated mice. Taken together, our findings suggest that mitochondrial abnormalities lie at the center of VIDD pathogenesis, leading us to propose a novel paradigm for VIDD in which metabolic oversupply could act as a key instigator of mitochondrial dysfunction and oxidative stress in the mechanically ventilated diaphragm. Some of the results of these studies have been previously reported in the form of abstracts (26–28).

METHODS

Human Study Subjects

Diaphragm and biceps muscle specimens were removed from brain-dead organ donors who had undergone MV (MV group, n = 11) for variable periods of time; the biopsies were surgically obtained in the operating room before circulatory arrest and organ harvest and immediately frozen in liquid nitrogen (for biochemical and molecular analyses) or cooled isopentane (for histology). Controls consisted of diaphragm samples obtained from age-matched patients during thoracic surgery for benign or malignant lung nodules (n = 15), and biceps biopsies from individuals with muscle complaints who were subsequently declared to be normal (n = 7). The biceps from patients with MV was used as an internal control muscle to account for any medication or other nonspecific effects of critical illness on skeletal muscle properties.

Histochemical, Biochemical, Microscopic, and Molecular Analyses

The online supplement contains details regarding ethics approval, reagents, mitochondrial enzymatic activity assays in muscle homogenates, RNA extraction and real-time quantitative polymerase chain reaction (qPCR), gene expression profile analysis, total lipid quantification and lipid droplet confocal imaging, *in situ* histochemical detection of respiratory chain deficiency, single-cell mtDNA deletion analyses, Western blotting including protein carbonyl measurements, and electron microscopy methods. A complete listing of DNA primers and probes used in the study is also available in the online supplement (*see* Tables E3 and E4).

Mouse MV Studies

Wild-type and Prx-3 transgenic (29) mice (all C57BL/6 background) underwent MV for 6 hours under general anesthesia as detailed in the online supplement, and contractile force measurements of the diaphragm were performed as previously described (30). A subset of mice were injected with the hyperlipidemia-inducing drug P407 (31) 24 hours before MV.

Statistical Analysis

Means ± SEM are presented for all data, and statistical methods are detailed in the online supplement. Because of limited amounts of biopsy material, certain analyses could not be performed in all human subjects, and the number of subjects for each variable is specifically indicated in each figure legend. The Mann-Whitney test was applied to compare groups in most cases unless stated otherwise, with statistical significance set at P less than 0.05.

RESULTS

Characteristics of Human Study Subjects

The clinical and demographic characteristics of the MV and control group subjects are shown in Tables E1 and E2. None of the control group subjects had experienced weight loss or other systemic manifestations of illness before surgery. The biceps was used as a nonrespiratory and nonweightbearing control muscle in both groups to ascertain whether changes in muscle properties associated with MV were specific to the diaphragm. There were no significant differences in the mean ages of the MV cohort (55 ± 5 yr) and the control diaphragm (58 ± 4 yr; $P = 0.86$) or control biceps (47 ± 3 yr; $P = 0.13$) subjects. The MV cohort was mechanically ventilated for an average period of 57 ± 13 hours (range, 15–176 h), whereas MV in control subjects was limited to the duration of surgery (range, 2–3 h).

Mitochondrial Impairment and Reduced Mitochondrial Biogenesis in Human MV Diaphragms

Impaired mitochondrial function was present in MV diaphragms, as indicated by reduced activity levels of the respiratory chain enzymes cytochrome-*c* oxidase (COX) and succinate dehydrogenase (SDH) (Figures 1A and 1B). The mitochondrial matrix enzyme citrate synthase, a marker of mitochondrial content, also tended to be decreased in MV diaphragms (Figure 1C).

The changes in COX and SDH were specific to the diaphragm, because activity levels of these enzymes did not differ significantly between MV and control subjects in the biceps muscle (Figures 1D–1F). Diaphragmatic COX and SDH values were normalized to citrate synthase to determine whether their reduced activity could be attributed to a lower mitochondrial content. After making this adjustment, COX activity remained significantly lower in MV diaphragms, whereas SDH activity did not differ from control subjects (Figures 1G and 1H). This suggests that mitochondrial impairment in MV diaphragms involved intrinsic enzymatic dysfunction of COX.

Muscle oxidative capacity is controlled by transcriptional coactivators, such as peroxisome proliferator activated receptor-γ coactivator (PGC)-1α and PGC-1β, which in turn act on downstream targets, such as mitochondrial transcriptional factor A (TFam). As one potential mechanism for mitochondrial abnormalities in MV diaphragms, several genes encoding proteins that promote mitochondrial biogenesis by acting on either nuclear DNA (Figure 2A) or mtDNA (Figure 2B) were found to be down-regulated. Other factors responsible for mitochondrial dynamics (fusion and fission), which are essential for proper functioning and mtDNA integrity, were also reduced (Figure 2C). As shown by the broader transcriptome (mRNA) analysis for each of the individual subjects in Figure 2D, a clear distinction in gene expression signatures was apparent between MV and control diaphragms. Although most mitochondrial and related metabolic genes were down-regulated in the MV group, notable exceptions consisted of mitochondrial superoxide dismutase (SOD2), the protein translation inhibitor EIF4EBP1, and adipokines (adiponectin and leptin), all of which showed a pattern of up-regulation in most subjects with MV.

Lipid Accumulation and Metabolic Oversupply in Human MV Diaphragms

To further dissect the nature of the above metabolic disturbances, muscle sections were incubated with oil red O to assess lipid content. This revealed that the diaphragm, and to a smaller extent the biceps, contained a higher lipid content in the patients with MV (Figures 3A and 3B; *see* Figure E1). Although myofiber atrophy may have contributed to an increase in the muscle fiber volume occupied by lipids (Figures 3C–3E), there was also an increased average size of individual lipid droplets (Figure 3F). Furthermore, transcript levels for fatty acid synthase and adipokines were also higher in MV group diaphragms, whereas muscle carnitine palmitoyl transferase-1, a transporter of fatty acids into mitochondria, was down-regulated in the MV group (Figures 3G and 3H).

Increased lipid accumulation within MV diaphragms could indicate an increased influx of metabolic substrates into muscle fibers relative to energetic consumption. Therefore, to evaluate cellular energy balance, we examined the two major intracellular metabolic sensor systems, AMP-activated protein kinase (AMPK) (Figures 3I–3L; see Figure E2) and sirtuin (SIRT)

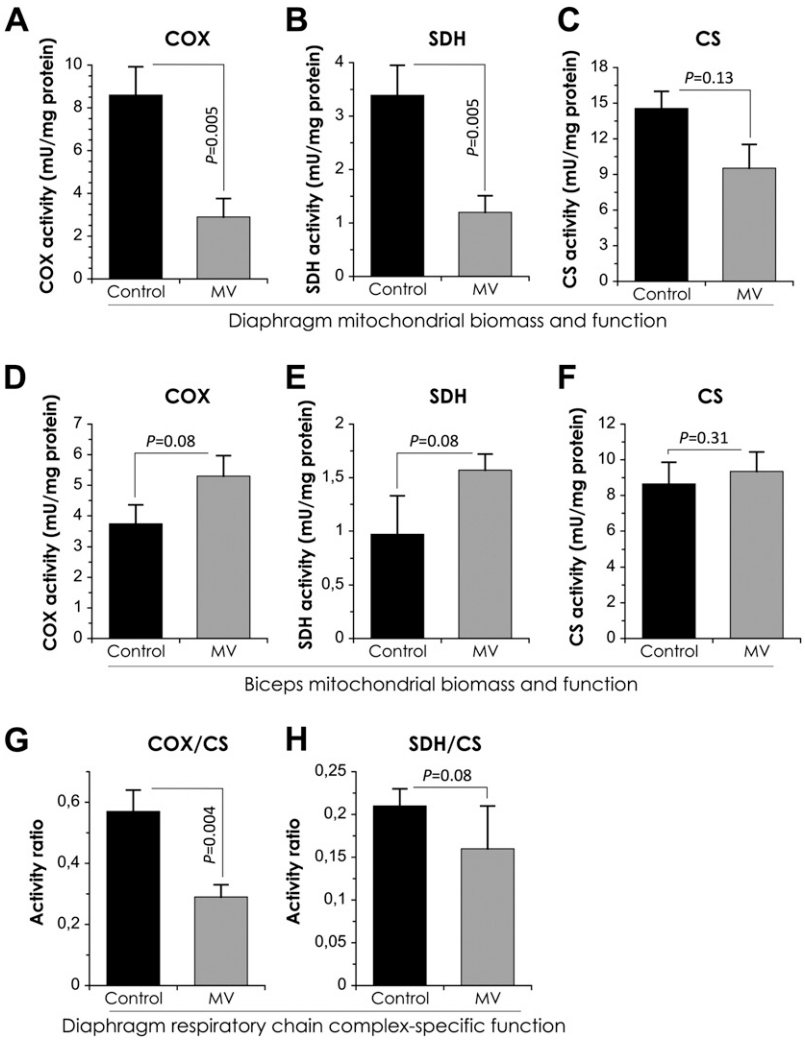

Figure 1. Reduced mitochondrial biomass and intrinsic respiratory chain dysfunction in human mechanically ventilated (MV) diaphragms. Enzymatic activity levels reflective of mitochondrial content and intrinsic respiratory chain functionality, determined in whole muscle homogenates, are shown for (*A* and *D*) mitochondrial cytochrome-*c* oxidase (COX), (*B* and *E*) succinate dehydrogenase (SDH), and (*C* and *F*) citrate synthase (CS). Mitochondrial respiratory chain complex–specific activities, as normalized to CS to adjust for mitochondrial content, are shown for (*G*) COX (complex IV) and (*H*) SDH (complex II). *A–C*, *G*, and *H* indicate data from MV and control group diaphragms; n = 11 per group. *D–F* show data from MV and control group biceps; n = 7–10 per group. Data are means ± SEM.

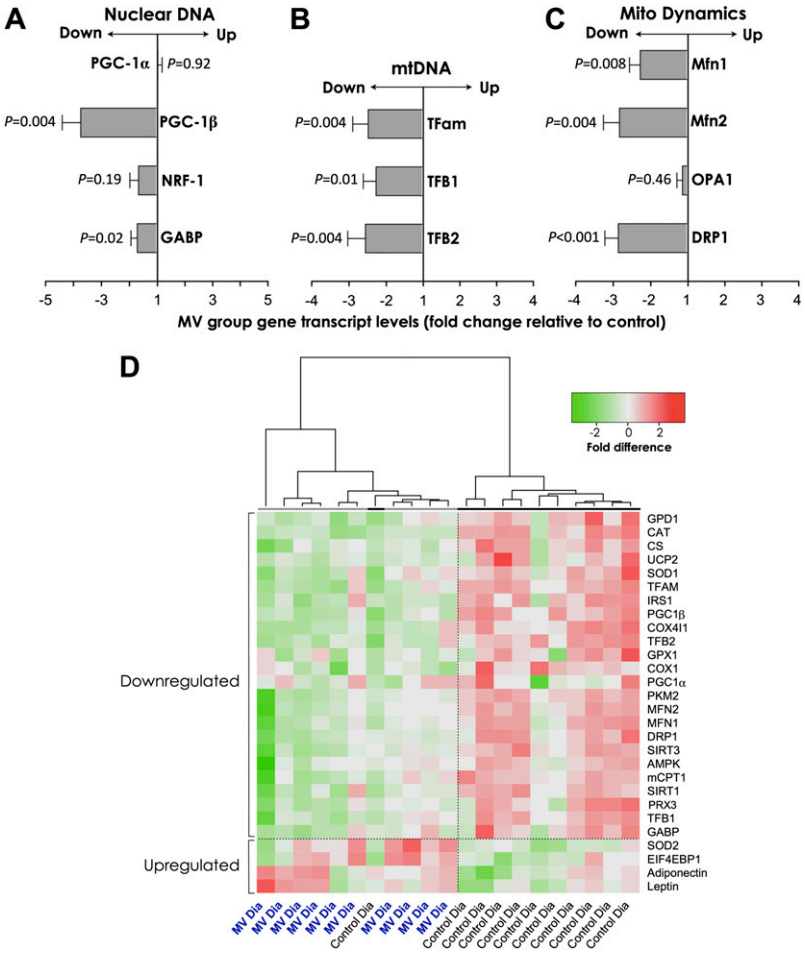

Figure 2. Impaired mitochondrial biogenesis in human mechanically ventilated (MV) diaphragms. Real-time quantitative polymerase chain reaction quantification of mRNA transcripts for key effectors of mitochondrial biogenesis acting on (*A*) nuclear DNA, (*B*) mitochondrial DNA, and (*C*) mitochondrial network dynamics; n = 10 for MV group, 7–11 for control subjects. (*D*) Heatmap of gene expression data with an unsupervised hierarchical clustering analysis of differentially expressed ($P < 0.05$) genes in diaphragms from control subjects and subjects with MV. The dendrogram atop the heatmap depicts the degree of similarity (*shorter vertical lines* indicating greater similarity) of gene expression profiles between individuals. Data are means ± SEM. AMPK = AMP-activated protein kinase; CAT = catalase; CS = citrate synthase; COX1 = cytochrome-*c* oxidase subunit 1; COX4I1 = cytochrome-*c* oxidase subunit 4 isoform 1; mCPT1 = carnitine palmitoyltransferase 1; DRP = dynamin-related protein; EIF4EBP1 = eukaryotic translation initiation factor 4E binding protein 1; GABP = GA binding protein transcription factor subunit-α; GPD = glycerol-3-phosphate dehydrogenase; GPX = glutathione peroxidase; IRS = insulin receptor substrate; Mfn = mitofusin; NRF = nuclear respiratory factor; OPA= optic atrophy; PGC = peroxisome proliferator activated receptor-γ coactivator; PKM2 = pyruvate kinase muscle isozyme; Prx-3 = peroxiredoxin 3; SIRT = sirtuin; SOD = superoxide dismutase; TFam, TFB1, TFB2 = mitochondrial transcription factors A, B1, and B2; UCP = uncoupling protein.

1 and 3 (Figures 3M and 3N), which are down-regulated under conditions of energetic oversupply. In MV diaphragms, absolute levels of active (phosphorylated) AMPK protein were significantly lower than in control diaphragms. The mRNA levels for SIRT1 and SIRT3 (a mitochondrial sirtuin), which are implicated in antioxidant functions, mitochondrial biogenesis, and fatty acid oxidation, were similarly lower in the MV diaphragms. These findings, together with increased intracellular lipid, suggest the possible development of a state of energetic substrate oversupply in diaphragm muscle fibers when their workload is taken over by the ventilator.

Mitochondrial DNA Damage in Human MV Diaphragm Muscle Fibers

Oxidative stress is known to play a central role in the pathogenesis of VIDD, and mitochondria-derived ROS in particular have the potential to directly damage mitochondrial components, including mtDNA. In patients with myopathies resulting specifically from mtDNA deletions, double-staining of muscle fibers to assess SDH and COX activities *in situ* reveals a characteristic pattern, in which SDH (entirely encoded by nuclear DNA) staining is preserved, whereas COX (partially encoded by mtDNA) is absent. Such SDH-positive and COX-negative fibers were present at abnormally high levels in diaphragms from patients with MV (Figures 4A–4C; *see* Figure E3). To ascertain whether mtDNA deletions were indeed present within these fibers, two different approaches were used (Figure 4D). First, mtDNA from muscle homogenates was subjected to long-range PCR, demonstrating different PCR products consistent with multiple mtDNA deletions (Figure 4E). Second, COX-negative and COX-positive fibers were individually isolated from MV diaphragms using laser capture microdissection (Figure 4F), and assayed using multiplex qPCR directed against a region spanning the mitochondrial nicotinamide adenine dinucleotide reduced dehydrogenase (ND)-1 and ND-4 genes. This assay confirmed a significantly greater prevalence of mtDNA deletions in COX-negative fibers (Figure 4G; *see* Figure E4). Finally, given that mtDNA is particularly vulnerable to damage from mitochondria-derived ROS, we also quantified the transcript levels of antioxidant enzymes, which were generally down-regulated (Figure 4H). However, of the two major mitochondrial antioxidants, SOD2 was up-regulated, whereas peroxiredoxin-3 (Prx-3), a mitochondria-specific scavenger of peroxides, demonstrated significant down-regulation in MV diaphragms.

Metabolic Oversupply and Mitochondrial Oxidative Stress during MV in Mice

To further probe the functional significance of metabolic substrate oversupply or mitochondria-derived oxidative stress during MV, we next examined responses in mouse models. In wild-type mice the development of VIDD was rapid, with significantly reduced force-generating capacity of the diaphragm after 6 hours of MV (Figure 5A). Oxidative stress was evaluated by measuring carbonylated proteins, which were increased approximately sevenfold over control levels in the MV diaphragms (Figure 5B). As in humans, these changes were associated with increased lipid accumulation within MV diaphragms

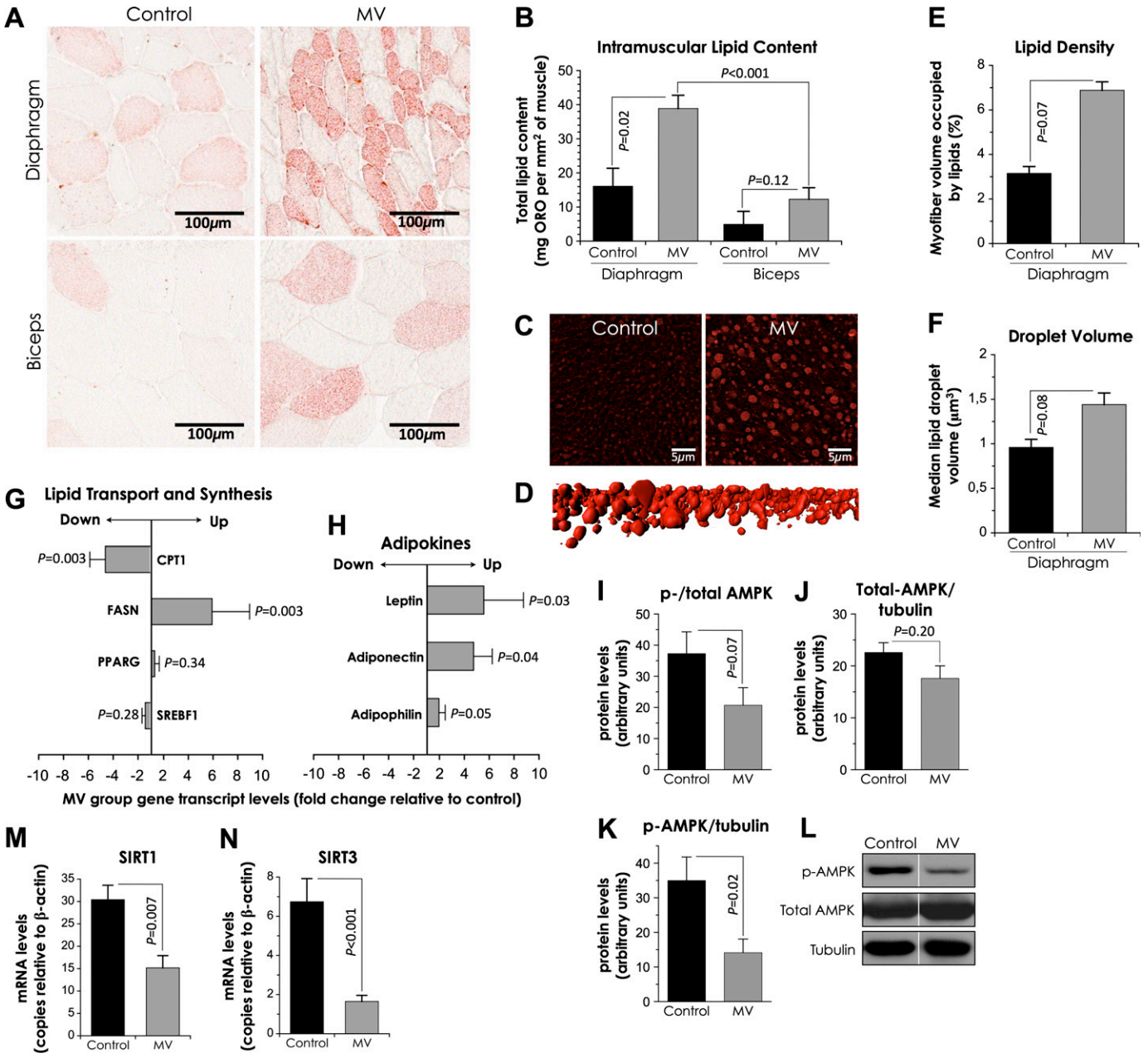

Figure 3. Increased lipid accumulation and metabolic oversupply in human mechanically ventilated (MV) diaphragms. (*A*) Oil red O lipid staining of diaphragm and biceps muscle sections from control subjects and individuals with MV. (*B*) Quantification of global intramuscular lipid content; n = 9–10 subjects for MV group, n = 4–6 for control subjects. (*C*) Confocal imaging of oil red O–stained muscle. (*D*) Three-dimensional reconstruction to quantify intramyocellular lipid droplet (*E*) density and (*F*) volume; n = 3 per group. (*G*) Real-time polymerase chain reaction quantification of mRNA levels of key genes associated with lipid transport and synthesis, and (*H*) lipid content (adipokines); n = 10 for MV group, n = 11 for control subjects. (*I*) Phosphorylation (activation) status of the cellular energy sensor and inducer of mitochondrial biogenesis, AMP-activated protein kinase (AMPK), relative to total AMPK levels; (*J*) total AMPK levels relative to the housekeeping gene tubulin; (*K*) phosphorylated AMPK levels relative to tubulin; and (*L*) representative immunoblot image (n = 7 per group; all samples were run on the same gel for a given protein as shown in Figure E2). (*M*) Real-time polymerase chain reaction quantification of mRNA levels for sirtuin (SIRT) 1, and (*N*) SIRT3; n = 10–11 per group. Data are presented as means ± SEM. CPT1 = muscle carnitine palmitoyltransferase 1; FASN = fatty acid synthase; PPARG = peroxisome proliferator activated receptor-γ; SREBF1 = sterol regulatory element binding factor 1.

(Figures 5C and 5D). Next, the drug P407 was used to induce an acute and reproducible hyperlipidemic state, to increase lipid substrate availability to the diaphragm during MV (*see* Figure E5). This tended to further suppress diaphragmatic force ($P = 0.054$) during MV (Figure 5E), and was also associated with a greater level of oxidative stress in the diaphragm (Figure 5F). Finally, to more specifically evaluate the role of mitochondria-derived oxidative stress in VIDD, we used transgenic mice overexpressing Prx-3, an antioxidant that is only present within mitochondria, and which is down-regulated in human MV diaphragms. Importantly, Prx-3 mice maintained normal diaphragmatic force production (Figure 5G), whereas carbonylated proteins in the diaphragm increased less than threefold (Figure 5H) after MV, thus supporting a

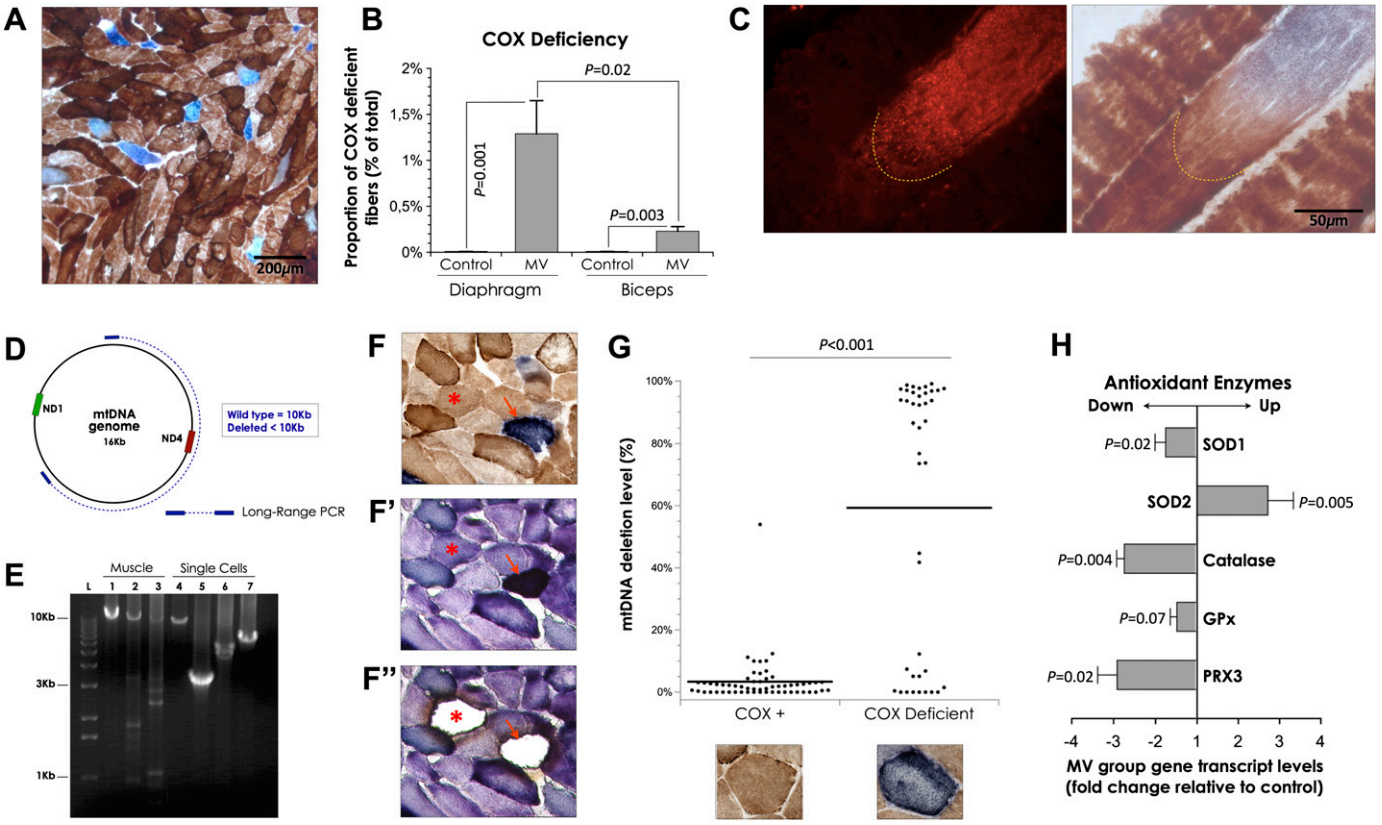

Figure 4. Muscle fibers with cytochrome-*c* oxidase (COX) selective respiratory chain deficiency and mitochondrial DNA deletions in human mechanically ventilated (MV) diaphragms. (*A*) Muscle sections were sequentially stained for COX and succinate dehydrogenase (SDH) activity: *blue-staining* cells indicate respiratory chain deficiency selectively affecting COX. (*B*) The proportion of COX-deficient cells in COX-SDH–stained muscle sections was quantified by manually counting over 88,000 cells; n = 8–9 for MV diaphragms and biceps, n = 7–8 for control subjects. (*C*) Triple stained oil red O, COX, SDH muscle section visualized with epifluorescence (*left*, lipid droplets) and bright field (*right*, COX-SDH). (*D*) The major arc of the mtDNA genome was screened for deletions by long-range polymerase chain reaction (LR-PCR) in whole-muscle homogenates and single cells. Full length (no deletion) product is 10 kb. (*E*) LR-PCR products resolved by agarose gel electrophoresis. Lanes 1–3: LR-PCR products of whole-muscle homogenates from subjects with MV (lower-molecular-weight products suggest mtDNA deletions in Lanes 2–3). Lanes 4–7: LR-PCR products from a single COX-positive cell (Lane 4) and three COX-deficient cells (Lanes 5–7) with lower-molecular-weight PCR products consistent with mtDNA deletions (L = ladder). Note that the presence of a DNA fragment less than 10 kb in Lane 7, despite the absence of detectable deletion by the real-time nicotinamide adenine dinucleotide reduced [NADH] dehydrogenase (ND)1/ND4 qPCR assay, indicates that not all deletions involved the ND4 gene region. (*F*) COX-positive (*brown*, example denoted by *asterisk*) and COX-deficient (*blue*, example denoted by *arrow*) cells were identified by double COX-SDH staining, and (*F′*) sections stained with SDH only were used for (*F″*) laser capture microdissection of single cells of each type. (*G*) Collected single muscle cells of either COX-positive (n = 57) or COX-deficient (n = 41) phenotype were individually screened for the common mtDNA ND4 deletion using the multiplex real-time qPCR ND1/ND4 assay. *Horizontal bars* represent means of each group (3.4 ± 1% for COX-positive, 59.3 ± 6.7% for COX-deficient). (*H*) Real-time qPCR quantification of mRNA transcript levels for the antioxidant enzymes copper-zinc superoxide dismutase (SOD1), manganese SOD (SOD2), catalase, glutathione peroxidase (GPx), and mitochondrial peroxiredoxin (PRX3); n = 10–11 per group. Data are means ± SEM.

major role for mitochondria-derived ROS in the pathogenesis of VIDD.

DISCUSSION

Diaphragmatic strength and endurance are critical determinants of the ability to successfully remove patients from MV (1, 3). Here we provide evidence that MV is associated with multiple changes in metabolic function of the diaphragm consisting of (*1*) mitochondrial respiratory chain deficiency, with a loss of COX enzymatic activity that is disproportionately large relative to reductions in mitochondrial content; (*2*) a generalized down-regulation in the expression of mitochondrial biogenesis and antioxidant factors; (*3*) mitochondrial genome damage, as indicated by the presence of mtDNA deletions; and (*4*) signs of metabolic oversupply including increased lipid accumulation within diaphragmatic muscle fibers. Furthermore, through the use of a transgenic mouse model, we demonstrate that overexpression of an antioxidant specifically localized within mitochondria (Prx-3) completely abrogates the loss of diaphragmatic force-generating capacity, which defines the VIDD phenomenon. Thus, in the human and murine models, our data suggest that adverse alterations in mitochondrial function represent a critical pathophysiologic link between MV and ensuing diaphragmatic impairment.

Adequate mitochondrial function is a prerequisite for normal muscle oxidative capacity, and mitochondrial respiratory chain deficiency caused by mtDNA mutations is a known cause of exercise intolerance in humans (32, 33). The mitochondrial genome seems to be particularly vulnerable to ROS-induced DNA damage (34). Complex II (SDH) is entirely encoded by the nuclear genome, whereas several complex IV (COX) subunits are encoded by mtDNA. SDH activity did not differ between MV and control diaphragms after normalization to account for the reduced

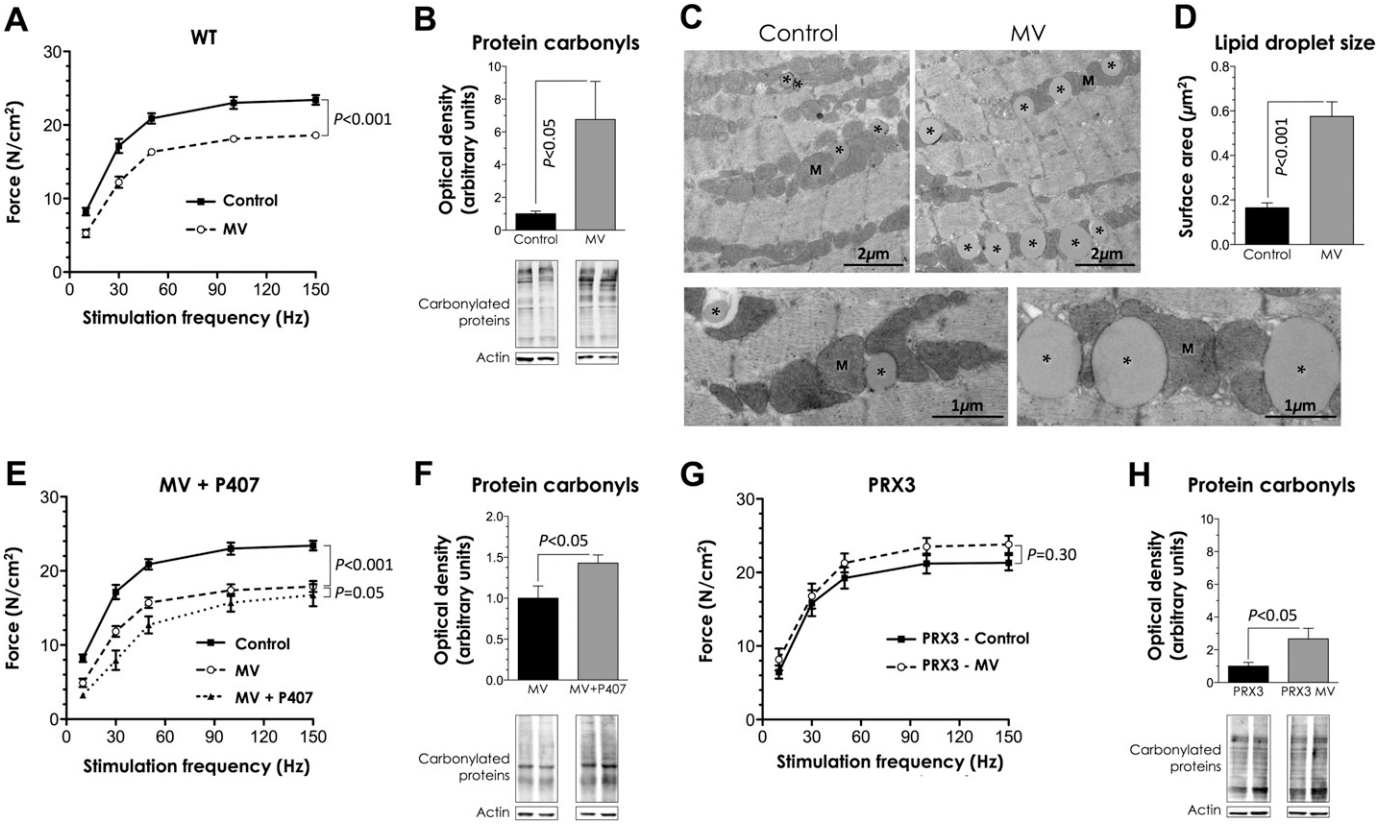

Figure 5. Effects of hyperlipidemia and transgenic overexpression of a mitochondria-specific antioxidant on ventilator-induced diaphragmatic dysfunction in mice. After wild-type (WT) mice were mechanically ventilated (MV) for 6 hours, (*A*) diaphragmatic contractile force was reduced and (*B*) diaphragmatic protein carbonylation (oxidative stress) was increased approximately sevenfold. In addition, electron microscopy revealed an increased size of lipid droplets (*asterisks*) in MV diaphragms (*C* and *D*), which were often found in close proximity to mitochondria (M). The changes in (*E*) diaphragmatic contractility and (*F*) oxidative stress were exacerbated by the induction of hyperlipidemia with P407 treatment in WT mice. In transgenic mice overexpressing peroxiredoxin 3 (PRX3) exposed to MV for 6 hours, (*G*) diaphragmatic force production remained normal and (*H*) oxidative stress increased less than threefold. Data are means ± SEM. n = 5 per group for contractility; n = 4 per group for protein carbonylation.

mitochondrial content found in the MV group. In contrast, a persistent deficiency of about 50% in COX activity was observed, and the COX-SDH costaining pattern in MV diaphragms (i.e., COX deficiency with maintenance of SDH staining) is further evidence for a specific impairment of mtDNA encoded subunits (35). This pattern is characteristic of patients with hereditary mutations of complex IV and other mitochondrial diseases associated with mtDNA deletions (35–37). It is also found at a much lower level in some elderly individuals (37, 38), in whom COX-deficient fibers are believed to reflect an increased proportion of mutant mtDNA copies resulting from cumulative oxidative stress-induced damage (39). An interesting aspect of mtDNA-mutated mitochondria is the ability to undergo local clonal expansion within individual fiber segments (40, 41). Such segmental COX deficiency was found in several diaphragm muscle fibers of the MV group, and the prevalence of COX-deficient fibers was also higher in older patients with MV (*see* Figures E6 and E7). However, it should be noted that although the increased presence of mtDNA deletions in human MV diaphragms may be caused by greater mitochondria-derived ROS, this remains to be determined.

Previous work in animal models and humans has shown that oxidative modifications are prominent in MV diaphragms (14, 42, 43). Our findings are consistent with these data, because mitochondria with deficient respiratory chain function can permit excessive electron leakage with consequent increases in ROS production (44). Oxidative stress has the potential to inhibit contractile mechanisms directly, and is also pivotal in triggering several proteolytic pathways implicated in muscle atrophy (9, 43). Mitochondrial biogenesis is generally accompanied by an up-regulation of antioxidant mechanisms (45). Therefore, the down-regulation of transcriptional regulators of mitochondrial biogenesis genes may explain the apparent inability of MV diaphragms to up-regulate antioxidant defenses. Only the mitochondria-specific isoform of SOD2 demonstrated a compensatory up-regulation in MV group diaphragms, which is in keeping with a mitochondrial source of oxidative stress (10, 11). However, increased SOD2 expression in MV diaphragms did not prevent respiratory chain deficiency and mtDNA damage. This may be because the end-product of SOD2 activity, H_2O_2, could not be effectively removed due to the substantial down-regulation of catalase and Prx-3 expression levels in MV diaphragms. Indeed, although SOD2 relieves mitochondrial oxidative stress caused by superoxide, it also generates increased levels of H_2O_2 that can damage macromolecules including mtDNA (46). Such an explanation is supported by the fact that transgenic overexpression of Prx-3 (29), a mitochondria-specific scavenger of H_2O_2, allowed for preservation of diaphragmatic force production after MV in mice.

Although our findings and those of others (10, 11, 42) establish the existence of mitochondrial functional abnormalities in MV diaphragms, an important question remains: what is the primary cellular stimulus for these events? There has been much recent interest in the relationship between metabolic

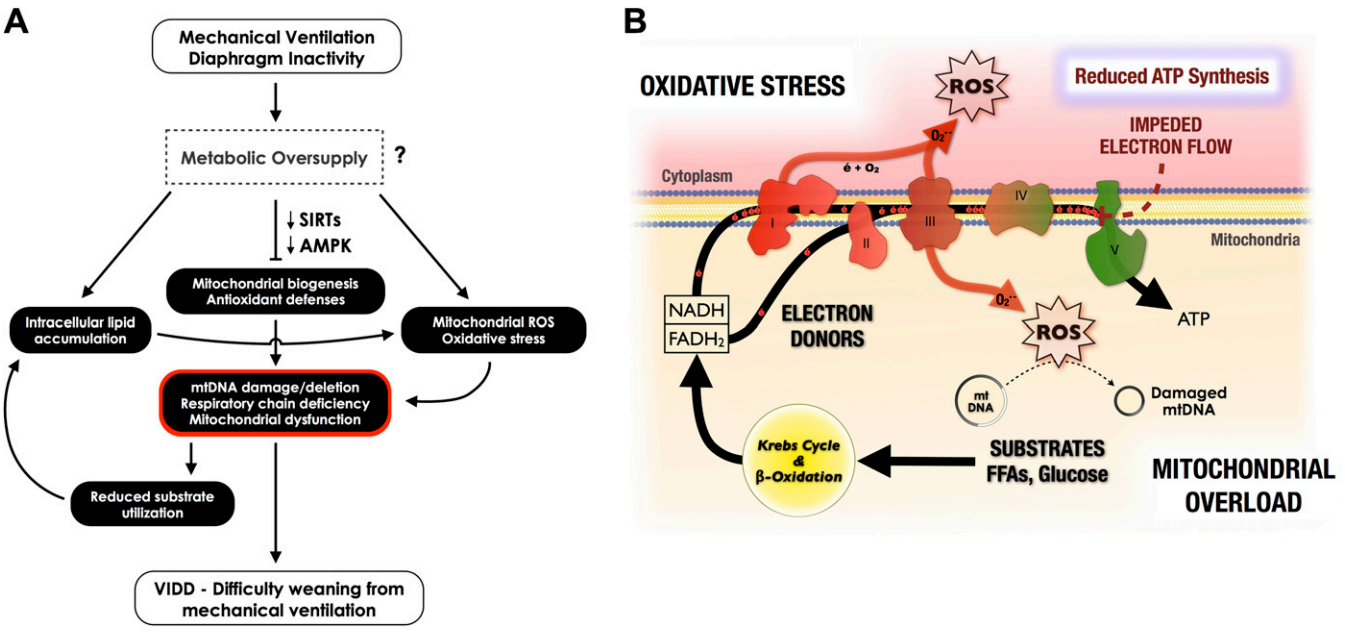

Figure 6. Proposed mechanistic scheme for diaphragmatic dysfunction during mechanical ventilation (MV). (*A*) Reduced contractile activity of the diaphragm during MV alters the energetic balance in the muscle, resulting in decreased mitochondrial biogenesis and enzymatic activity, with increased lipid accumulation and oxidative stress, the latter leading to mitochondrial DNA (mtDNA) damage. These changes compromise contractile function of the diaphragm during attempts at weaning from MV. (*B*) Under normal conditions in which there is appropriate metabolic balance in the diaphragm, electrons derived from energetic substrates are freely shuttled down the electron transport chain, as shown by the *main arrow* representing the driving force for electron flow. However, when energetic substrate supply greatly exceeds metabolic demand, electron flow is inhibited. This can be associated with reduced ATP synthesis and increased leakage of surplus electrons from the electron transport chain (mitochondrial overload). These surplus electrons can then react with surrounding molecular oxygen, leading to increased reactive oxygen species (ROS) generation from mitochondria (Complexes I and III). AMPK = AMP-activated protein kinase; p-AMPK = phosphorylated (activated) AMPK; SIRTs = sirtuins1 and 3; FFAs = free fatty acids; VIDD = ventilator-induced diaphragmatic dysfunction.

oversupply and increased mitochondrial ROS production as a cause of insulin resistance in the metabolic syndrome and type 2 diabetes (15, 18, 21). An excess of intracellular energetic substrates relative to ATP demand leads to a build-up of electron donors (i.e., NADH, $FADH_2$) generated from the tricarboxylic acid (Krebs) cycle and β-oxidation pathway (15). Under such conditions of "mitochondrial overload" (18), electron flow down the respiratory chain is impeded, and this is associated with an increased probability of electrons leaking and interacting with molecular oxygen to form superoxide (15, 24). Furthermore, to the extent that metabolic oversupply is associated with increased intramyocellular lipids, the latter can react with ROS and themselves become potent sources of oxidative stress (lipotoxicity) (47), thus propagating the cycle of free radical generation and mitochondrial dysfunction (48). Our finding that intracellular lipid accumulation, COX deficiency, and mtDNA deletions can colocalize (see Figure 4C) is consistent with this notion. Indeed, exposure of muscle cells to saturated free fatty acids *in vitro* induces ROS-dependent mtDNA damage (23).

MV causes a sudden interruption of diaphragmatic contractile activity, such that the energetic requirements of the muscle are abruptly reduced. Because one of the main criteria for brain death is an absence of spontaneous respiratory activity, it can be assumed that patients with MV in our study lacked significant respiratory muscle activation for most of their intensive care unit stay. To determine whether a state of energetic oversupply might exist in the diaphragms of these patients, we examined the responses of two master sensors of cellular energy status, AMPK and SIRT1. AMPK is activated by increases in the intracellular AMP/ATP ratio, whereas SIRTs are nicotinamide adenine dinucleotide–dependent deacetylases (49). In the setting of energetic depletion, these two metabolic sensor systems are upregulated and synergize to promote mitochondrial biogenesis and fatty acid oxidation (50–53). Conversely, energetic oversupply is characterized by a functional down-regulation of AMPK and SIRTs 1/3. Accordingly, the decreases in activated AMPK and SIRT expression, reduction of mitochondrial biogenesis transcription factor expression (which can also be explained by suppression of AMPK and SIRT signaling) (49), and presence of ectopic lipid within muscle fibers are all highly suggestive of a state of metabolic oversupply in human diaphragms subjected to major inactivity as a result of MV.

These findings lead us to propose a new hypothesis regarding the pathogenesis of VIDD, in which metabolic oversupply could represent a primary initiating factor, because it is capable of unifying the elements of mitochondrial respiratory chain deficiency, mitochondria-derived oxidative stress, and abnormal lipid accumulation found within diaphragms exposed to sustained MV (Figure 6). To the extent that patients in the intensive care unit often have high serum levels of metabolic substrates, such as glucose and free fatty acids (54), this might further exacerbate the situation by increasing substrate availability to the diaphragm during MV. This idea is supported by our observation that induction of hyperlipidemia further increased oxidative stress and tended to worsen diaphragmatic function in the mouse diaphragm exposed to MV. Indeed, it is interesting to note that the early delivery of high caloric intake with parenteral nutrition was recently associated with a prolongation of weaning time (55), whereas intensive insulin therapy to prevent hyperglycemia has been reported to accelerate the weaning process (56).

Finally, certain methodologic limitations of our study should be addressed. First, our sample size was relatively small, and the

patients were heterogeneous in terms of past medical history. Second, many patients were transferred to our hospital from other institutions, and the ventilation mode before transfer was not always well documented. Third, patients in the control biceps cohort were different from the control diaphragm patients and tended to be younger, although the latter would be expected to exaggerate changes attributed to MV in the biceps and is thus unlikely to have affected our main conclusions. Finally, our study is not able to ascertain whether the preferential mitochondrial dysfunction and greater lipid accumulation observed after MV in the diaphragm (as compared with the nonrespiratory biceps muscle) results solely from MV-induced inactivity, or is also related to a greater intrinsic vulnerability of the diaphragm to systemic factors associated with critical illness. However, it should be noted that in either scenario, the ability to generate adequate intramuscular energy supplies upon a sudden resumption of diaphragmatic activity during weaning attempts would be impaired by the loss of mitochondrial function.

In summary, our findings suggest that MV is associated with the rapid development of metabolic dysregulation and mitochondrial respiratory chain deficiency in the human diaphragm, which may result at least in part from a state of energy substrate oversupply relative to demand in the muscle. Accordingly, clinical measures designed to restore metabolic balance in the diaphragm, such as reducing energetic substrate overload or increasing diaphragmatic contractile activity levels, should be useful in preventing these deleterious changes. Importantly, impaired mitochondrial function caused by metabolic oversupply can be rescued by activating the AMPK/PGC-1α signaling axis (57, 58), which simultaneously up-regulates mitochondrial biogenesis and antioxidant defenses (45, 50). Therefore, pharmacologic agents with the capacity to stimulate AMPK (e.g., metformin) (59) and SIRT agonists (e.g., resveratrol) (60), or mitochondria-targeted antioxidant therapies (10, 61), particularly if initiated early in the course of MV, could all potentially be valuable adjuncts for mitigating the adverse consequences of MV on diaphragmatic function.

Author disclosures are available with the text of this article at www.atsjournals.org.

Acknowledgment: The authors are indebted to the patients and their families for their willingness to participate in this study, and to the cooperation of Transplant Quebec in this project. They thank Tong Li, Christian Lemaire, Johanne Bourdon, Mullah Abu Shadeque, and Zia Saleh for technical contributions; Robert Guérin, Dr. Erin O'Ferrall, and Dr. John Richardson for expert opinion on histologic work; Dr. Eric Shoubridge, Dr. Robert Taylor, and Dr. Nicholas Bertos for use of their facility; Dr. Hana Antonicka, Dr. Gilles Gouspillou, Dr. Julie Murphy, and the MRG members for technical assistance; Kathyrn White and Tracey Davey (EM Research Services, Newcastle University) for assistance with the electron microscopy work; and Dr. Hana Antonicka and Dr. Russ Hepple for useful comments on the manuscript.

References

1. Vassilakopoulos T, Zakynthinos S, Roussos C. The tension-time index and the frequency/tidal volume ratio are the major pathophysiologic determinants of weaning failure and success. *Am J Respir Crit Care Med* 1998;158:378–385.
2. Hermans G, Agten A, Testelmans D, Decramer M, Gayan-Ramirez G. Increased duration of mechanical ventilation is associated with decreased diaphragmatic force: a prospective observational study. *Crit Care* 2010;14:R127.
3. Tobin MJ, Laghi F, Brochard L. Role of the respiratory muscles in acute respiratory failure of COPD: lessons from weaning failure. *J Appl Physiol* 2009;107:962–970.
4. Esteban A, Ferguson ND, Meade MO, Frutos-Vivar F, Apezteguia C, Brochard L, Raymondos K, Nin N, Hurtado J, Tomicic V, *et al*. Evolution of mechanical ventilation in response to clinical research. *Am J Respir Crit Care Med* 2008;177:170–177.
5. Powers SK, Kavazis AN, Levine S. Prolonged mechanical ventilation alters diaphragmatic structure and function. *Crit Care Med* 2009;37:S347–S353.
6. Levine S, Nguyen T, Taylor N, Friscia ME, Budak MT, Rothenberg P, Zhu J, Sachdeva R, Sonnad S, Kaiser LR, *et al*. Rapid disuse atrophy of diaphragm fibers in mechanically ventilated humans. *N Engl J Med* 2008;358:1327–1335.
7. Jaber S, Petrof BJ, Jung B, Chanques G, Berthet JP, Rabuel C, Bouyabrine H, Courouble P, Koechlin C, Sebbane M, *et al*. Rapidly progressive diaphragmatic weakness and injury during mechanical ventilation in humans. *Am J Respir Crit Care Med* 2010;183:364–371.
8. Vassilakopoulos T, Petrof BJ. Ventilator-induced diaphragmatic dysfunction. *Am J Respir Crit Care Med* 2004;169:336–341.
9. Petrof BJ, Jaber S, Matecki S. Ventilator-induced diaphragmatic dysfunction. *Curr Opin Crit Care* 2010;16:19–25.
10. Powers SK, Hudson MB, Nelson WB, Talbert EE, Min K, Szeto HH, Kavazis AN, Smuder AJ. Mitochondria-targeted antioxidants protect against mechanical-ventilation-induced diaphragm weakness. *Crit Care Med* 2011;39:1749–1759.
11. Tang H, Lee M, Budak MT, Pietras N, Hittinger S, Vu M, Khuong A, Hoang CD, Hussain SN, Levine S, *et al*. Intrinsic apoptosis in mechanically ventilated human diaphragm: linkage to a novel fos/foxo1/stat3-bim axis. *FASEB J* 2011;25:2921–2936.
12. Zergeroglu MA, McKenzie MJ, Shanely RA, Van Gammeren D, DeRuisseau KC, Powers SK. Mechanical ventilation-induced oxidative stress in the diaphragm. *J Appl Physiol* 2003;95:1116–1124.
13. Whidden MA, McClung JM, Falk DJ, Hudson MB, Smuder AJ, Nelson WB, Powers SK. Xanthine oxidase contributes to mechanical ventilation-induced diaphragmatic oxidative stress and contractile dysfunction. *J Appl Physiol* 2009;106:385–394.
14. Hussain SN, Mofarrahi M, Sigala I, Kim HC, Vassilakopoulos T, Maltais F, Bellenis I, Chaturvedi R, Gottfried SB, Metrakos P, *et al*. Mechanical ventilation-induced diaphragm disuse in humans triggers autophagy. *Am J Respir Crit Care Med* 2010;182:1377–1386.
15. Anderson EJ, Lustig ME, Boyle KE, Woodlief TL, Kane DA, Lin CT, Price JW III, Kang L, Rabinovitch PS, Szeto HH, *et al*. Mitochondrial H_2O_2 emission and cellular redox state link excess fat intake to insulin resistance in both rodents and humans. *J Clin Invest* 2009;119:573–581.
16. Yu T, Sheu SS, Robotham JL, Yoon Y. Mitochondrial fission mediates high glucose-induced cell death through elevated production of reactive oxygen species. *Cardiovasc Res* 2008;79:341–351.
17. Balaban RS, Nemoto S, Finkel T. Mitochondria, oxidants, and aging. *Cell* 2005;120:483–495.
18. Koves TR, Ussher JR, Noland RC, Slentz D, Mosedale M, Ilkayeva O, Bain J, Stevens R, Dyck JR, Newgard CB, *et al*. Mitochondrial overload and incomplete fatty acid oxidation contribute to skeletal muscle insulin resistance. *Cell Metab* 2008;7:45–56.
19. Petersen KF, Dufour S, Befroy D, Garcia R, Shulman GI. Impaired mitochondrial activity in the insulin-resistant offspring of patients with type 2 diabetes. *N Engl J Med* 2004;350:664–671.
20. Muoio DM, Newgard CB. Mechanisms of disease: molecular and metabolic mechanisms of insulin resistance and beta-cell failure in type 2 diabetes. *Nat Rev Mol Cell Biol* 2008;9:193–205.
21. Houstis N, Rosen ED, Lander ES. Reactive oxygen species have a causal role in multiple forms of insulin resistance. *Nature* 2006;440:944–948.
22. Medikayala S, Piteo B, Zhao X, Edwards JG. Chronically elevated glucose compromises myocardial mitochondrial DNA integrity by alteration of mitochondrial topoisomerase function. *Am J Physiol Cell Physiol* 2011;300:C338–C348.
23. Rachek LI, Musiyenko SI, LeDoux SP, Wilson GL. Palmitate induced mitochondrial deoxyribonucleic acid damage and apoptosis in L6 rat skeletal muscle cells. *Endocrinology* 2007;148:293–299.
24. Hoehn KL, Salmon AB, Hohnen-Behrens C, Turner N, Hoy AJ, Maghzal GJ, Stocker R, Van Remmen H, Kraegen EW, Cooney GJ, *et al*. Insulin resistance is a cellular antioxidant defense mechanism. *Proc Natl Acad Sci USA* 2009;106:17787–17792.
25. Palmeira CM, Rolo AP, Berthiaume J, Bjork JA, Wallace KB. Hyperglycemia decreases mitochondrial function: the regulatory role of mitochondrial biogenesis. *Toxicol Appl Pharmacol* 2007;225:214–220.
26. Jung B, Mrozek S, Petrof BJ, Lacampagne A, Matecki S, Jaber S. Ventilator-induced diaphragmatic dysfunction: development and perspectives of the first mouse model. *Am J Respir Crit Care Med* 2011;183:A4245.
27. Picard M, Liang F, Hussain SN, Goldberg AL, Danialou G, Chaturvedi R, Matecki S, Jaber S, Des Rosiers C, Karpati G, *et al*. Mitochondrial

dysfunction and lipid accumulation in the human diaphragm during mechanical ventilation. *Am J Respir Crit Care Med* 2011;183:A4257.
28. Jung B, Azuelos I, Li T, Liang F, Okazaki T, Picard M, Pauly M, Jaber S, Petrof BJ. Overexpression of peroxiredoxin-3, prevents ventilator-induced diaphragmatic dysfunction in mice. Preliminary results. *Am J Respir Crit Care Med* 2012;185:A2705.
29. Matsushima S, Ide T, Yamato M, Matsusaka H, Hattori F, Ikeuchi M, Kubota T, Sunagawa K, Hasegawa Y, Kurihara T, *et al*. Overexpression of mitochondrial peroxiredoxin-3 prevents left ventricular remodeling and failure after myocardial infarction in mice. *Circulation* 2006;113:1779–1786.
30. Divangahi M, Balghi H, Danialou G, Comtois AS, Demoule A, Ernest S, Haston C, Robert R, Hanrahan JW, Radzioch D, *et al*. Lack of CFTR in skeletal muscle predisposes to muscle wasting and diaphragm muscle pump failure in cystic fibrosis mice. *PLoS Genet* 2009;5:e1000586.
31. Johnston TP. The p-407–induced murine model of dose-controlled hyperlipidemia and atherosclerosis: a review of findings to date. *J Cardiovasc Pharmacol* 2004;43:595–606.
32. Taivassalo T, Gardner JL, Taylor RW, Schaefer AM, Newman J, Barron MJ, Haller RG, Turnbull DM. Endurance training and detraining in mitochondrial myopathies due to single large-scale mtDNA deletions. *Brain* 2006;129:3391–3401.
33. Taivassalo T, Jensen TD, Kennaway N, DiMauro S, Vissing J, Haller RG. The spectrum of exercise tolerance in mitochondrial myopathies: a study of 40 patients. *Brain* 2003;126:413–423.
34. Yakes FM, Van Houten B. Mitochondrial DNA damage is more extensive and persists longer than nuclear DNA damage in human cells following oxidative stress. *Proc Natl Acad Sci USA* 1997;94:514–519.
35. Taylor RW, Turnbull DM. Mitochondrial DNA mutations in human disease. *Nat Rev Genet* 2005;6:389–402.
36. Murphy JL, Blakely EL, Schaefer AM, He L, Wyrick P, Haller RG, Taylor RW, Turnbull DM, Taivassalo T. Resistance training in patients with single, large-scale deletions of mitochondrial DNA. *Brain* 2008;131:2832–2840.
37. Taylor RW, Schaefer AM, Barron MJ, McFarland R, Turnbull DM. The diagnosis of mitochondrial muscle disease. *Neuromuscul Disord* 2004; 14:237–245.
38. Muller-Hocker J. Cytochrome-*c* oxidase deficient fibres in the limb muscle and diaphragm of man without muscular disease: an age-related alteration. *J Neurol Sci* 1990;100:14–21.
39. Krishnan KJ, Reeve AK, Samuels DC, Chinnery PF, Blackwood JK, Taylor RW, Wanrooij S, Spelbrink JN, Lightowlers RN, Turnbull DM. What causes mitochondrial DNA deletions in human cells? *Nat Genet* 2008;40:275–279.
40. Chinnery PF, Howel D, Turnbull DM, Johnson MA. Clinical progression of mitochondrial myopathy is associated with the random accumulation of cytochrome-*c* oxidase negative skeletal muscle fibres. *J Neurol Sci* 2003;211:63–66.
41. Bender A, Krishnan KJ, Morris CM, Taylor GA, Reeve AK, Perry RH, Jaros E, Hersheson JS, Betts J, Klopstock T, *et al*. High levels of mitochondrial DNA deletions in substantia nigra neurons in aging and Parkinson disease. *Nat Genet* 2006;38:515–517.
42. Kavazis AN, Talbert EE, Smuder AJ, Hudson MB, Nelson WB, Powers SK. Mechanical ventilation induces diaphragmatic mitochondrial dysfunction and increased oxidant production. *Free Radic Biol Med* 2009;46:842–850.
43. Whidden MA, Smuder AJ, Wu M, Hudson MB, Nelson WB, Powers SK. Oxidative stress is required for mechanical ventilation-induced protease activation in the diaphragm. *J Appl Physiol* 2010;108:1376–1382.
44. Indo HP, Davidson M, Yen HC, Suenaga S, Tomita K, Nishii T, Higuchi M, Koga Y, Ozawa T, Majima HJ. Evidence of ROS generation by mitochondria in cells with impaired electron transport chain and mitochondrial DNA damage. *Mitochondrion* 2007;7:106–118.
45. St-Pierre J, Drori S, Uldry M, Silvaggi JM, Rhee J, Jager S, Handschin C, Zheng K, Lin J, Yang W, *et al*. Suppression of reactive oxygen species and neurodegeneration by the PGC-1 transcriptional coactivators. *Cell* 2006;127:397–408.
46. Lee HY, Choi CS, Birkenfeld AL, Alves TC, Jornayvaz FR, Jurczak MJ, Zhang D, Woo DK, Shadel GS, Ladiges W, *et al*. Targeted expression of catalase to mitochondria prevents age-associated reductions in mitochondrial function and insulin resistance. *Cell Metab* 2010;12: 668–674.
47. Schrauwen P, Schrauwen-Hinderling V, Hoeks J, Hesselink MK. Mitochondrial dysfunction and lipotoxicity. *Biochim Biophys Acta* 2010; 1801:266–271.
48. Bugger H, Abel ED. Molecular mechanisms for myocardial mitochondrial dysfunction in the metabolic syndrome. *Clin Sci (Lond)* 2008; 114:195–210.
49. Canto C, Gerhart-Hines Z, Feige JN, Lagouge M, Noriega L, Milne JC, Elliott PJ, Puigserver P, Auwerx J. AMPK regulates energy expenditure by modulating NAD+ metabolism and Sirt1 activity. *Nature* 2009;458:1056–1060.
50. Handschin C, Spiegelman BM. The role of exercise and PGC1alpha in inflammation and chronic disease. *Nature* 2008;454:463–469.
51. Canto C, Auwerx J. PGC-1alpha, Sirt1 and AMPK, an energy sensing network that controls energy expenditure. *Curr Opin Lipidol* 2009;20: 98–105.
52. Lin SJ, Ford E, Haigis M, Liszt G, Guarente L. Calorie restriction extends yeast life span by lowering the level of NADH. *Genes Dev* 2004;18:12–16.
53. Canto C, Jiang LQ, Deshmukh AS, Mataki C, Coste A, Lagouge M, Zierath JR, Auwerx J. Interdependence of AMPK and Sirt1 for metabolic adaptation to fasting and exercise in skeletal muscle. *Cell Metab* 2010;11:213–219.
54. Zaloga GP, Willey S, Tomasic P, Chernow B. Free fatty acids alter calcium binding: a cause for misinterpretation of serum calcium values and hypocalcemia in critical illness. *J Clin Endocrinol Metab* 1987; 64:1010–1014.
55. Casaer MP, Mesotten D, Hermans G, Wouters PJ, Schetz M, Meyfroidt G, Van Cromphaut S, Ingels C, Meersseman P, Muller J, *et al*. Early versus late parenteral nutrition in critically ill adults. *N Engl J Med* 2011;365:506–517.
56. Hermans G, Wilmer A, Meersseman W, Milants I, Wouters PJ, Bobbaers H, Bruyninckx F, Van den Berghe G. Impact of intensive insulin therapy on neuromuscular complications and ventilator dependency in the medical intensive care unit. *Am J Respir Crit Care Med* 2007;175:480–489.
57. Kukidome D, Nishikawa T, Sonoda K, Imoto K, Fujisawa K, Yano M, Motoshima H, Taguchi T, Matsumura T, Araki E. Activation of AMP-activated protein kinase reduces hyperglycemia-induced mitochondrial reactive oxygen species production and promotes mitochondrial biogenesis in human umbilical vein endothelial cells. *Diabetes* 2006;55:120–127.
58. Viscomi C, Bottani E, Civiletto G, Cerutti R, Moggio M, Fagiolari G, Schon EA, Lamperti C, Zeviani M. In vivo correction of Cox deficiency by activation of the AMPK/PGC-1alpha axis. *Cell Metab* 2011; 14:80–90.
59. Kane DA, Anderson EJ, Price JW III, Woodlief TL, Lin CT, Bikman BT, Cortright RN, Neufer PD. Metformin selectively attenuates mitochondrial H_2O_2 emission without affecting respiratory capacity in skeletal muscle of obese rats. *Free Radic Biol Med* 2010;49:1082–1087.
60. Timmers S, Konings E, Bilet L, Houtkooper RH, van de Weijer T, Goossens GH, Hoeks J, van der Krieken S, Ryu D, Kersten S, *et al*. Calorie restriction-like effects of 30 days of resveratrol supplementation on energy metabolism and metabolic profile in obese humans. *Cell Metab* 2011;14:612–622.
61. Camara AK, Lesnefsky EJ, Stowe DF. Potential therapeutic benefits of strategies directed to mitochondria. *Antioxid Redox Signal* 2010;13: 279–347.

ONLINE SUPPLEMENT

Mitochondrial Dysfunction and Lipid Accumulation in the Human Diaphragm during Mechanical Ventilation

Martin Picard, Boris Jung, Feng Liang, Ilan Azuelos, Sabah Hussain, Peter Goldberg, Richard Godin, Gawiyou Danialou, Rakesh Chaturvedi, Karolina Rygiel, Stefan Matecki, Samir Jaber, Christine Des Rosiers, George Karpati, Lorenzo Ferri, Yan Burelle, Douglass M Turnbull, Tanja Taivassalo and Basil J. Petrof

Table of Contents

Supplemental Figure S1.

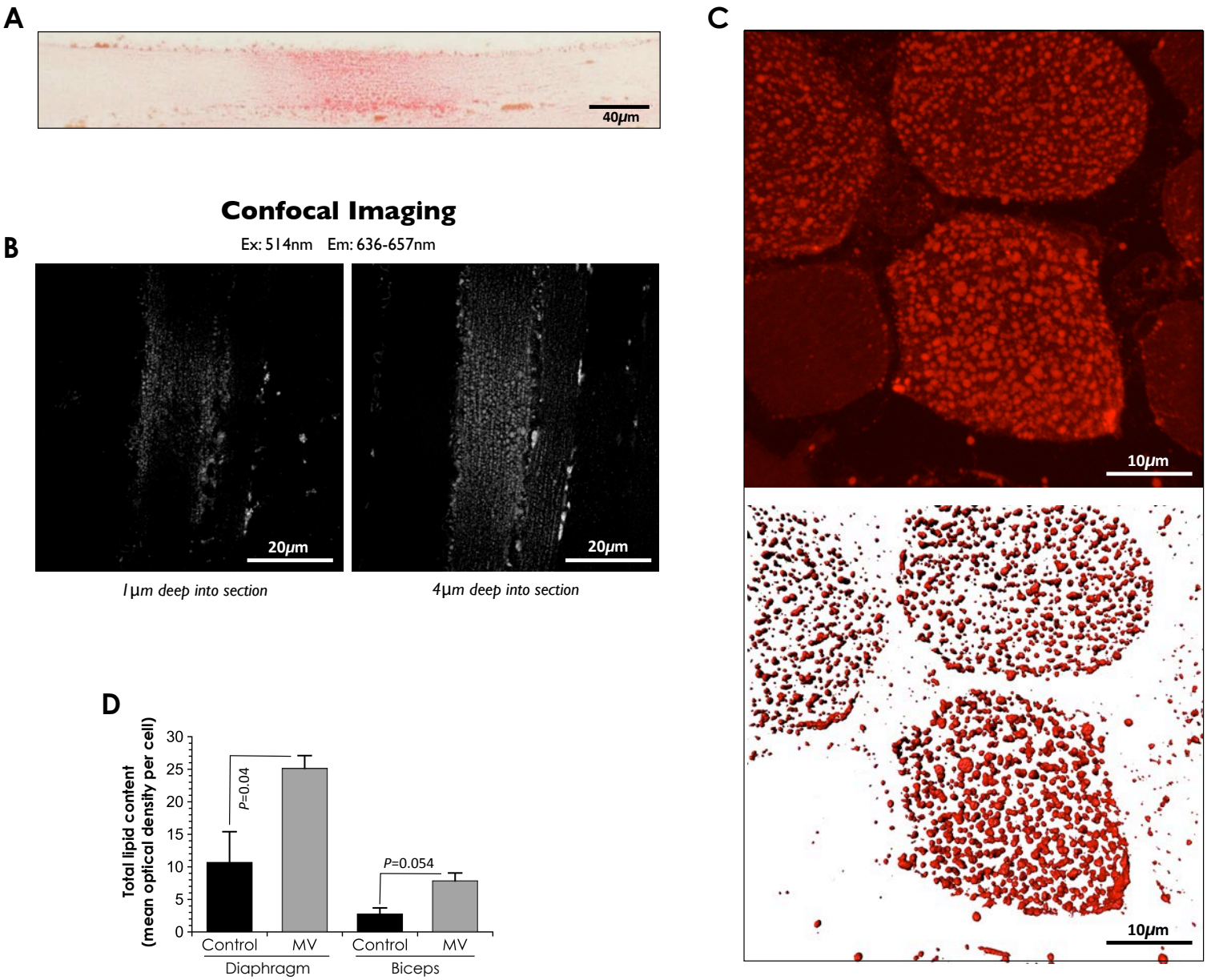

Intramyocellular lipid droplet accumulation is segmental and occurs preferentially in the diaphragm. (**A**) Single cell in longitudinal section from MV diaphragm muscle stained with Oil-red-O. (**B**) Confocal microscopy images of a longitudinal section taken at different depths of a region demonstrating the segmental nature of lipid accumulation and the preferential subsarcolemmal accumulation of lipid droplets. Images were acquired as described in the **Supplemental Methods.** (**C**) Raw confocal image (top) and 3D reconstruction (bottom) used to determine myofiber lipid droplet density. (**D**) Intracellular lipid content assessed by optical density quantification of ~200 individual fibers per subject stained with Oil-red-O, as described in the **Supplemental Methods**. n = 7-10 per group for diaphragms and 5-9 for biceps; values are means ± S.E.M.

Supplemental Figure S2.

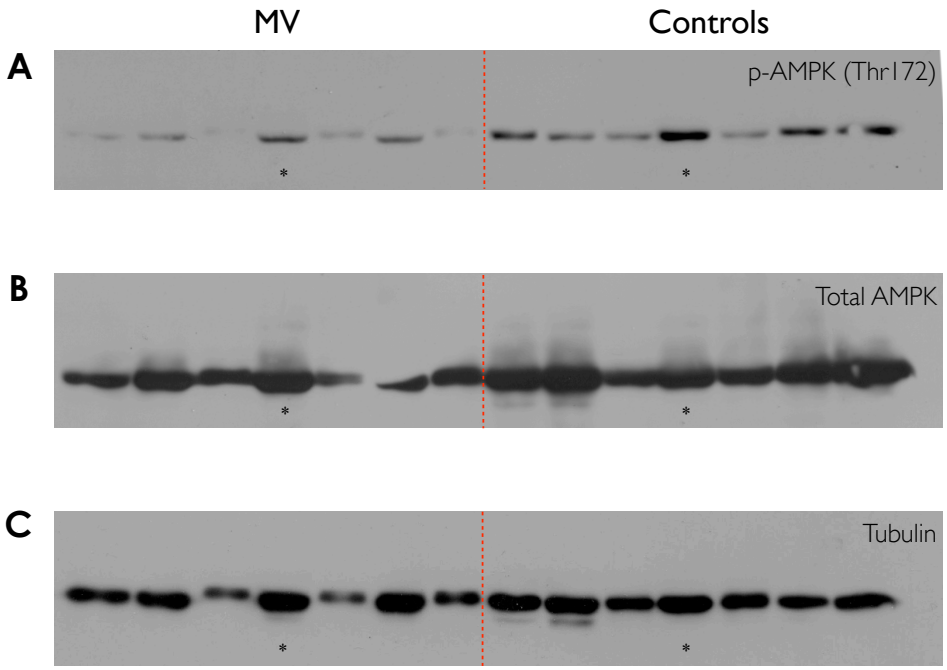

Whole immunoblots for AMP-activated protein kinase (AMPK) content and phosphorylation status in mechanically ventilated (MV) and control diaphragms. Immunoblots are shown for (**A**) phosphorylated AMPK (p-AMPK) at Thr172, (**B**) total AMPK levels and (**C**) tubulin. ***** designates samples shown in main Figure 3L.

Supplemental Figure S3.

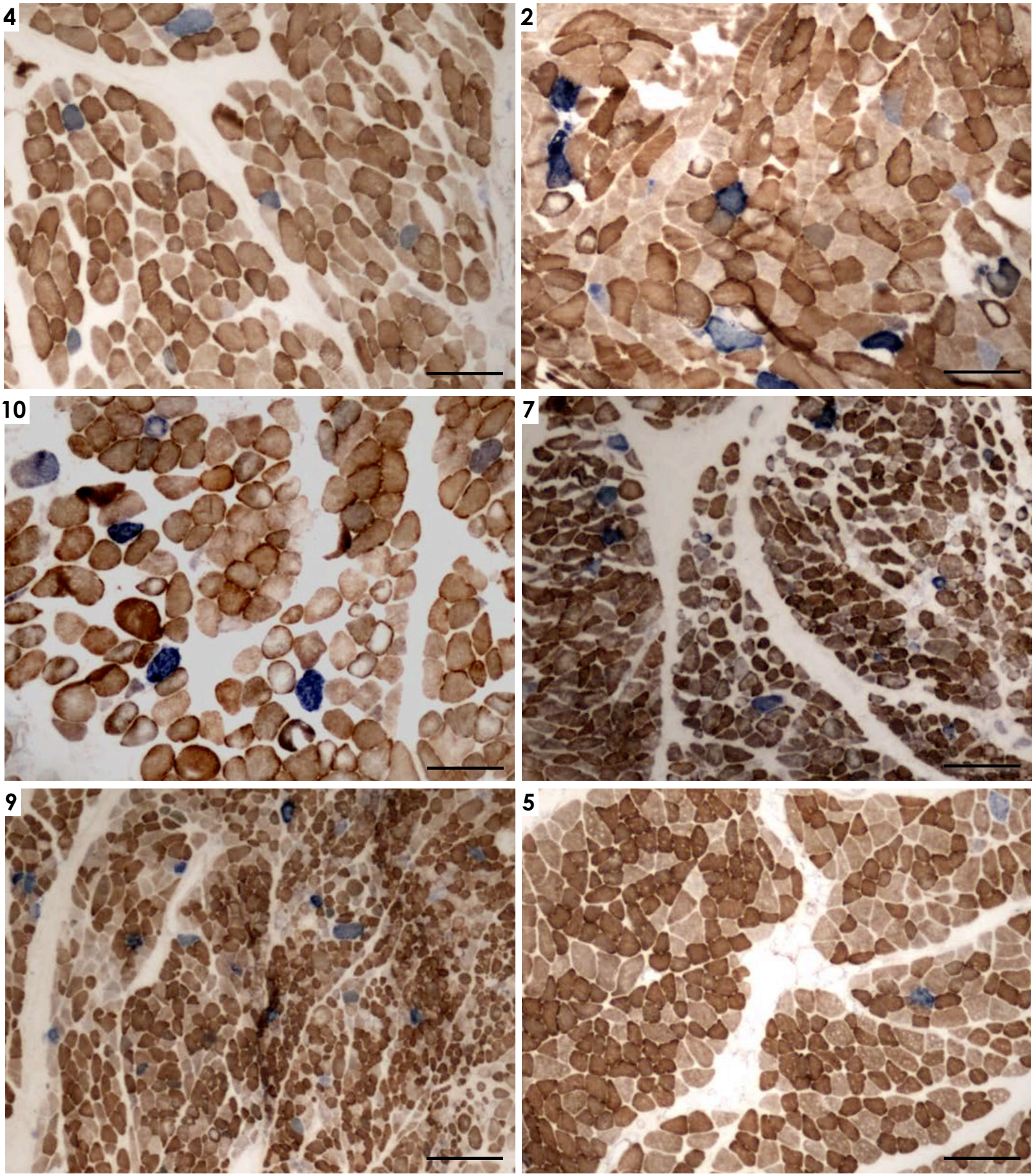

Respiratory chain deficiency detected by dual COX/SDH histochemical staining. Shown are diaphragm sections from MV subjects showing COX deficiency. Blue fibers (SHD staining) are visible due to the absence of COX staining in some muscle fibers. Image numbers correspond to subjects numbers in **Supplemental Table S1**. Scale bars represent 200μm.

Supplemental Figure S4.

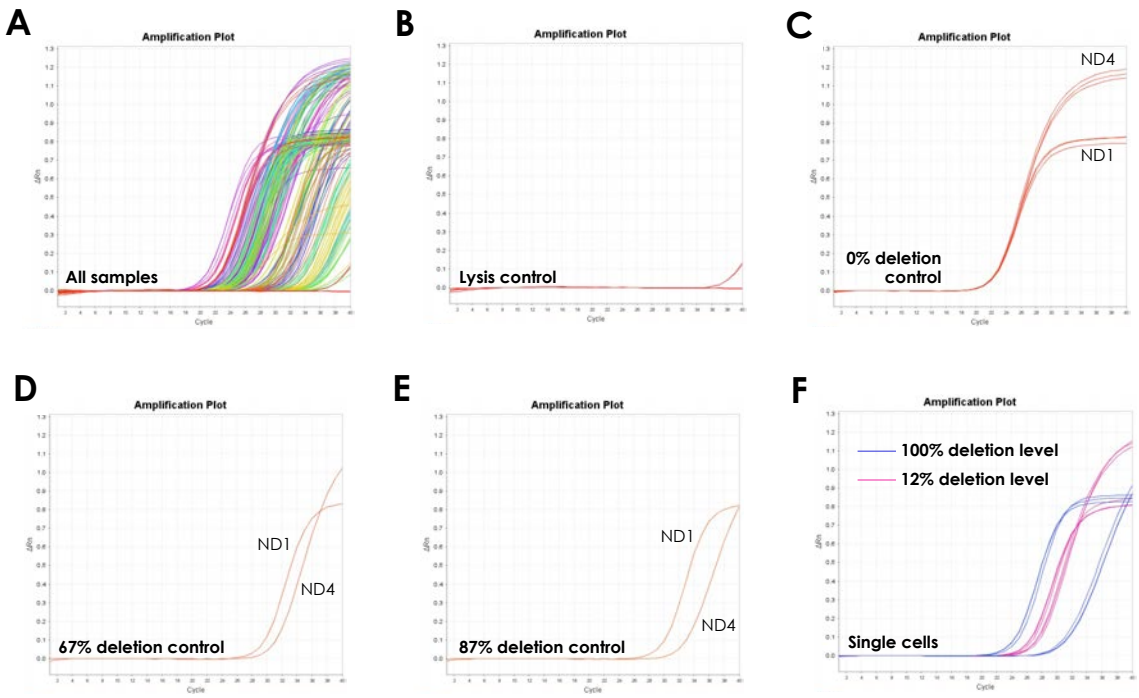

Real-time PCR amplification plots for ND1/ND4 mutiplex mtDNA deletion assay. Mitochondrial DNA (mtDNA) from single cells was amplified by real-time PCR and fluorescence of probes specific to ND1 and ND4 was measured at the end of each amplification cycle. Shown are amplification plots for (**A**) all samples of a single run, (**B**) lysis (negative) control containing only the lysis buffer for single cells, (**C**) control genomic DNA from blood sample known to harbor no mtDNA deletion, (**D**) control DNA from muscle known to harbor 67% deletion level, (**E**) control DNA from muscle known to harbor 87% deletion level, and (**F**) two single cells containing 100% and 12% deletion load, respectively. Deletion levels in controls were characterized by Southern Blotting. Sequences for primers and probes are listed in **Supplemental Table S4**.

Supplemental Figure S5.

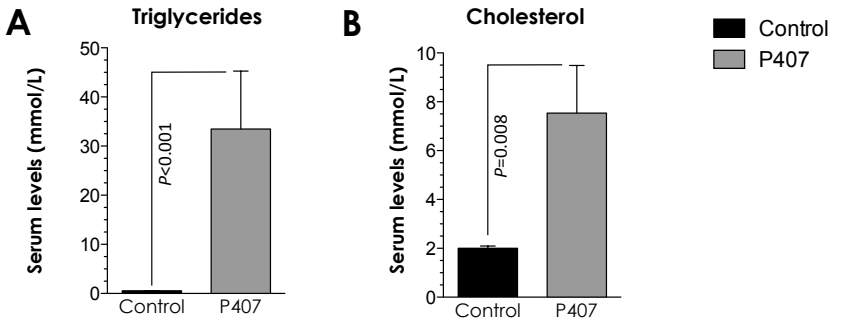

Effect of treatment with P407 on plasma triglycerides and cholesterol in mice. Blood lipid levels were measured 24 hours after treatment with P407. (**A**) Triglycerides and (**B**) cholesterol levels were increased 61.3-fold and 3.8-fold with P407, respectively. Shown are means ± S.E.M; n = 5 animals per group.

Supplemental Figure S6.

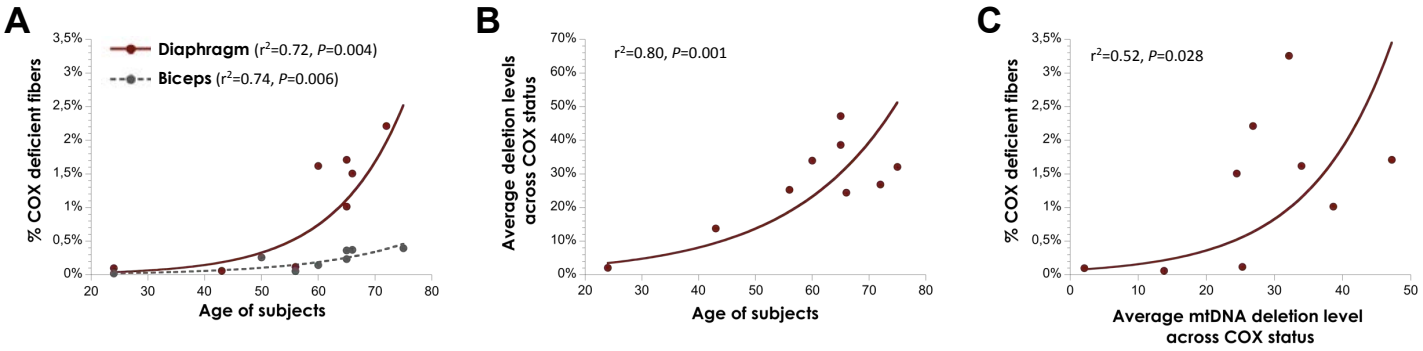

Advanced age is associated with higher deletion level and COX deficiency in mechanically ventilated diaphragms. (**A**) Exponential correlation between subject age and proportion of COX deficient cells detected histochemically. No COX deficient fibers were found in diaphragm or biceps muscles of controls processed under the same conditions. (**B**) Exponential correlation between subjects age and average mtDNA deletion levels calculated as the compound mean of deletion levels in i) COX positive, ii) COX intermediate and ii) COX negative fibers. (**C**) Exponential correlation between average mtDNA deletion levels and proportion of COX deficiency detected histochemically.

Supplemental Figure S7.

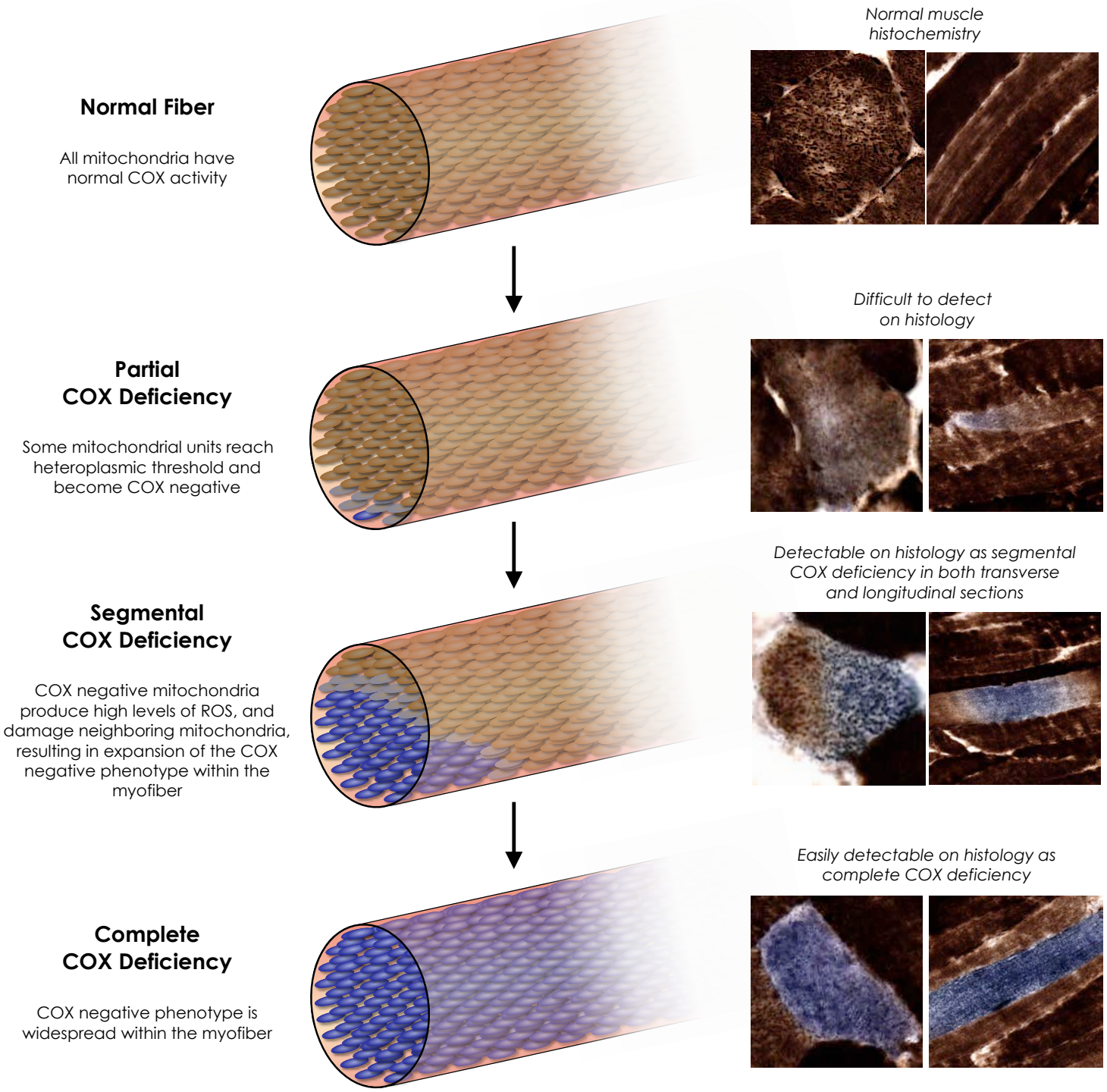

Proposed model underlying the development of segmental mitochondrial respiratory chain deficiency in diaphragm muscle fibers during mechanical ventilation. Images on the right represent muscle fibers in transverse and longitudinal sections sequentially stained for COX and SDH activities. During mechanical ventilation, mitochondria generate increased levels of reactive oxygen species (ROS), which induce DNA damage and dysfunction within neighboring mitochondria. It is hypothesized that expansion of COX deficient segments within diaphragmatic muscle cells results from the combined effects of mtDNA damage and a failure to achieve compensatory upregulation of mitochondrial biogenesis and antioxidant mechanisms.

Supplemental Table S1. Demographic data and relevant medical history in all study subjects

Subject	Age (yr)	Sex	MV Duration (h)	Reason for Intervention	Relevant Medical History
MV Group Diaphragm and Biceps				**Cause of Brain Death**	
1	65	M	32.5	Cerebrovascular accident	Coronary artery disease, smoker
2	75	M	29	Cerebrovascular accident	Coronary artery disease
3	32	M	34	Cerebrovascular accident	Marijuana smoker
4	64	M	36	Cerebrovascular accident	Hyperlipidema
5	55	M	42	Cerebrovascular accident	Smoker
6	27	F	176	Pulmonary embolism	Tonsillectomy
7	60	F	66	Cerebrovascular accident	Osteoporosis, depression
8	44	F	93	Cerebrovascular accident	None
9	72	F	15	Cerebrovascular accident	Chest nodule, smoker
10	66	M	49.5	Aspiration, anoxic encephalopathy	Coronary artery disease
11	50	M	49	Head trauma secondary to motor vehicle accident	Diabetes
Control Group Diaphragm				**Reason for Surgery**	
1	48	M	2.5	Stage 1A adenocarcinoma of the lung	Smoker
2	44	M	2	Stage 1A adenocarcinoma of the lung	Diabetes, smoker
3	39	M	3	Stage 1A adenocarcinoma of the lung	Transient ischemic attack, smoker
4	54	M	2	Stage 1A adenocarcinoma of the lung	Obesity, smoker
5	61	M	2.5	Stage 1A adenocarcinoma of the lung	None
6	44	M	2	Stage 1A adenocarcinoma of the lung	Smoker
7	55	M	2	Stage 1A adenocarcinoma of the lung	Alcoholism, cirrhosis, smoker
8	65	M	2	Stage 1A adenocarcinoma of the lung	Larynx resection for carcinoma, smoker
9	65	M	3	Stage 1A adenocarcinoma of the lung	None
10	52	F	2	Stage 1A adenocarcinoma of the lung	Smoker
11	38	M	2	Stage 1A adenocarcinoma of the lung	Smoker
12	74	M	2	Stage 1A adenocarcinoma of the lung	Hypertension, diabetes
13	83	M	2	Pulmonary metastasis (colon cancer)	Coronary artery disease, smoker
14	73	F	2	Stage 2A squamous cell carcinoma of the lung	Coronary artery disease, smoker
15	74	F	2	Benign lung nodule	Hypertension, diabetes
Control Group Biceps				**Reason for Biopsy**	
1	49	M	0	Myalgias	Statin use
2	49	M	0	Rule out myotonica congenita	None
3	42	M	0	Muscle cramps	None
4	42	M	0	Rule out inflammatory myopathy	None
5	49	M	0	Myalgias	Coronary artery disease
6	62	F	0	Rule out inflammatory myopathy	None
7	33	M	0	Myalgias	None

Supplemental Table S2. Clinical and ventilatory support parameters for mechanically ventilated subjects

Subject		Blood pressure	pH	pO_2 (mmHg)	pCO_2 (mmHg)	HCO_3 (mmol/L)	FiO_2	MV Mode	Vt (ml)	PEEP (cmH_2O)	RR (breaths/min)
1	Initial	122/55	7.38	251	34	19.9	1.0	AC	600	5	20
	Final	100/65	7.49	114	31	20.3	0.6				
2	Initial	90/58	NA	NA	NA	NA	NA	CMV	700	5	12
	Final	100/40	7.43	217	26	16.7	0.5				
3	Initial	150/95	7.27	158	54	24.5	0.5	SIMV	600	5	14
	Final	120/75	7.41	444	39	24.2	1.0				
4	Initial	118/60	7.41	462	42	26	1.0	SIMV	600	5	12
	Final	126/64	7.37	441	43	24.9	1.0				
5	Initial	105/60	7.44	94	38	24.1	0.3	AC	640	8	12
	Final	122/60	7.42	83	37	23.9	0.5				
6	Initial	144/55	7.37	123	51	28	1.0	SIMV	700	5	14
	Final	121/71	7.37	190	45	26	1.0				
7	Initial	153/62	7.31	116	43	21	0.5	AC	550	5	12
	Final	110/45	7.33	415	43	21.9	1.0				
8	Initial	120/80	7.4	93	41	25.4	NA	CMV	675	5	10
	Final	120/80	7.34	219	40	21.6	1.0				
9	Initial	NA	NA	NA	NA	NA	NA	NA	NA	NA	NA
	Final	NA	NA	NA	NA	NA	NA				
10	Initial	85/50	7.31	104	46	23	0.5	AC	600	12	14
	Final	98/50	7.31	260	42	21	0.5				
11	Initial	146/87	7.41	306	32	20.3	0.5	AC	700	10	10
	Final	127/69	7.33	349	50	26.4	1.0				

Note : "Initial" refers to values on admission; "Final" refers to values immediately prior to organ harvest.

Abbreviations:
pO_2 = arterial partial pressure of O_2
PCO_2 = arterial partial pressure of CO_2
HCO_3 = bicarbonate concentration
FiO_2 = Fractional inspired oxygen
MV = Mechanical ventilation
AC = Assist control
CMV = Controlled mandatory ventilation
SIMV = Synchronized intermittent mandatory ventilation
Vt = Tidal volume
PEEP = Positive end expiratory pressure
RR = Respiratory rate
NA = Not available

Supplemental Table S3. Sequences of primers used for real-time quantitative PCR to determine mRNA levels

	Forward primer	Reverse primer
Adiponectin	5'-CCTGGTGAGAAGGGTGAGAA-3'	5'-CCTTTCCTGCCTTGGATTC-3'
Adipophilin	5'-CTGTGTGTGAGATGGCAGAG-3'	5'-AGCCCCTTACAGGCATAGGT-3'
AMPK2α	5'-GACGGGTTGAAGAGATGGAA-3'	5'-CCTGCATACAATCTGCCTGA-3'
Catalase	5'-CGATGGGAGTCTTCTTTCCA-3'	5'-TGTGCATGCTAAAGGAGCAG-3'
COX1	5'-TGGAGCCTCCGTAGACCTAA-3'	5'-AGGACGGATCAGACGAAGAG-3'
COX4I1	5'-ACAACCGTCTTCCACTCGTT-3'	5'-CCATGTCAAGCACCTGTCTG-3'
CPT1	5'-AGATGGCCATGCTGAGAAGT-3'	5'-CAACAGTGGGTTCCTCCTTC-3'
CS	5'-GCAGAAGGAAGTTGGCAAAG-3'	5'-CGCGGATCAGTCTTCCTTAG-3'
DRP1	5'-TGGAATAACCCTTCCCATCA-3'	5'-TATCCTCGCTGTCACTGCTG-3'
EIF4EBP1	* Commercial source of primers	* Commercial source of primers
FASN	5'-TGTGGATGGCCTGGTAGG-3'	5'-ACCGGCTCTCCTTCTTCTTC-3'
GABP	5'-AACGCCTTGGGATACCCTAT-3'	5'-CTCCCCGAAATGTTGAGTGT-3'
GPD1	* Commercial source of primers	* Commercial source of primers
GPX1	5'-CTCTTCGTTCTTGGCGTTCT-3'	5'-GGACTACACCCAGATGAACGA-3'
IRS1	* Commercial source of primers	* Commercial source of primers
Leptin	5'-CCAAACCGGTGACTTTCTGT-3'	5'-CCCATCCAAAAAGTCCAAGA-3'
Mfn1	5'-CGGAACTTGATCGAATAGCC-3'	5'-AGAGCTCTTCCCACTGCTTG-3'
Mfn2	5'-AGAGGCATCAGTGAGGTGCT-3'	5'-GCAGAACTTTGTCCCAGAGC-3'
NRF-1	5'-GGGGAAAGAAAGCTGCAAG-3'	5'-TGAAACCCTCTGCTTTTGCT-3'
OPA1	5'-GAAAGGGTCTGCTTGGTGAG-3'	5'-GCTTCTGTTGGGCATAGCTC-3'
PGC-1α	5'-GTGAAGACCAGCCTCTTTGC-3'	5'-AATCCGTCTTCATCCACAGG-3'
PGC-1β	5'-CCTGTGAGAGTGGGTGTGG-3'	5'-CCACTGTCAAGGTCTGCTCA-3'
PKM2	5'-CTCCTTCAAGTGCTGCAGTGGGG-3'	5'-TACAGGTGGGCCTGACGAGCTG-3'
PPARG	5'-GAGCCCAAGTTTGAGTTTGC-3'	5'-GGCGGTCTCCACTGAGAATA-3'
PRDX3	5'-GCCGTTGTCAATGGAGAGTT-3'	5'-TCCACTGAGACTGCGACAAC-3'
SIRT1	5'-GCGGGAATCCAAAGGATAAT-3'	5'-GCACCTAGGACATCGAGGAA-3'
SIRT3	5'-GCTTCTGCGGCTCTACACGCA-3'	5'-TCTGCCATCACGTCAGCCCGAA-3'
SOD1	5'-GAAGGTGTGGGGAAGCATTA-3'	5'-ACATTGCCCAAGTCTCCAAC-3'
SOD2	5'-GGGAGATGTTACAGCCCAGA-3'	5'-AGTCACGTTTGATGGCTTCC-3'
SREBF1	5'-CCCTGTAACGACCACTGTGA-3'	5'- ACAGTGGCTCCGTCTGTCTT-3'
Tfam	5'-GCTCAGAACCCAGATGCAA-3'	5'-CCGCCCTATAAGCATCTTGA-3'
TFB1	5'-CCAGGGGGAATCACAAGAT-3'	5'-TTCTCAGTTTCCCAGGTGCT-3'
TFB2	5'-AGATCCCGGAAATCCAGACT-3'	5'-CTACGCTTTGGGTTTTCCAG-3'
UCP2	5'-GAGGTGGTCGGAGATACCAA-3'	5'-CATAGGTCACCAGCTCAGCA-3'
β-Actin	5'-CTCTTCCAGCCTTCCTTCCT-3'	5'-AGCACTGTGTTGGCGTACAG-3'

* Primer sequences are proprietary (SABiosciences)

Supplemental Table S4. Sequences of primers and probes used for mtDNA analysis

Real-time ND1/ND4 multiplex assay (single cells deletion levels)	
ND1 – Forward Primer	5'- CCCTAAAACCCGCCACATCT -3'
ND1 – Reverse Primer	5'- GAGCGATGGTGAGAGCTAAGGT -3'
ND1 – Probe	5'- **VIC**-CCATCACCCTCTACATCACCGCCC**-TAMRA** -3'
ND4 – Forward Primer	5'- CCATTCTCCTCCTATCCCTCAAC -3'
ND4 – Reverse Primer	5'- CACAATCTGATGTTTTGGTTAAACTATATTT -3'
ND4 - Probe	5'- **FAM**-CCGACATCATTACCGGGTTTTCCTCTTG**-TAMRA** -3'
Long Range-PCR	
Forward Primer	5'-AGATTTACAGTCCAATGCTTC-3'
Reverse Primer	5'-AGATACTGCGACATAGGGTG-3'

ND1: NADH-dehydrogenase (mitochondrial respiratory chain complex I) subunit 1

ND4: NADH-dehydrogenase subunit 4

VIC: VIC fluorophore

FAM: 6-carboxyfluorescein fluorophore

TAMRA: tetramethylrhodamine quencher

Supplemental Table S5. Comparison of the effects of contractile inactivity and metabolic oversupply (diabetes) on molecular markers of mitochondrial biogenesis in skeletal muscle.

	Contractile inactivity	Refs.	Diabetes (oversupply)	Refs.	Mechanical ventilation (this study)
PGC-1α	Downregulated	(1, 2)	Unchanged (1) and downregulated (3,4)	(1, 3, 4)	Unchanged
PGC-1β	Unchanged	(1)	Downregulated	(3)	Downregulated
SIRT1	Downregulated	(5)	Downregulated	(6)	Downregulated
SIRT3	-	-	Downregulated	(7, 8)	Downregulated
Tfam	Downregulated	(2, 9)	Downregulated	(10)	Downregulated
Nrf1	Downregulated	(9)	Downregulated	(4)	Unchanged *

Notes: * Fold difference from control : -1.67, $P = 0.10$.

References

1. Timmons JA, Norrbom J, Scheele C, Thonberg H, Wahlestedt C, Tesch P. Expression profiling following local muscle inactivity in humans provides new perspective on diabetes-related genes. Genomics 2006;87:165-172.

2. Adhihetty PJ, O'Leary MF, Chabi B, Wicks KL, Hood DA. Effect of denervation on mitochondrially mediated apoptosis in skeletal muscle. J Appl Physiol 2007;102:1143-1151.

3. Zorzano A, Hernandez-Alvarez MI, Palacin M, Mingrone G. Alterations in the mitochondrial regulatory pathways constituted by the nuclear co-factors pgc-1alpha or pgc-1beta and mitofusin 2 in skeletal muscle in type 2 diabetes. Biochim Biophys Acta 2010;1797:1028-1033.

4. Patti ME, Butte AJ, Crunkhorn S, Cusi K, Berria R, Kashyap S, Miyazaki Y, Kohane I, Costello M, Saccone R, et al. Coordinated reduction of genes of oxidative metabolism in humans with insulin resistance and diabetes: Potential role of pgc1 and nrf1. Proc Natl Acad Sci U S A 2003;100:8466-8471.

5. Ringholm S, Bienso RS, Kiilerich K, Guadalupe-Grau A, Aachmann-Andersen NJ, Saltin B, Plomgaard P, Lundby C, Wojtaszewski JF, Calbet JA, et al. Bed rest reduces metabolic protein content and abolishes exercise-induced mrna responses in human skeletal muscle. Am J Physiol Endocrinol Metab 2011;301:E649-658.

6. de Kreutzenberg SV, Ceolotto G, Papparella I, Bortoluzzi A, Semplicini A, Dalla Man C, Cobelli C, Fadini GP, Avogaro A. Downregulation of the longevity-associated protein sirtuin 1 in insulin resistance and metabolic syndrome: Potential biochemical mechanisms. Diabetes 2010;59:1006-1015.

7. Jing E, Emanuelli B, Hirschey MD, Boucher J, Lee KY, Lombard D, Verdin EM, Kahn CR. Sirtuin-3 (sirt3) regulates skeletal muscle metabolism and insulin signaling via altered

mitochondrial oxidation and reactive oxygen species production. Proc Natl Acad Sci U S A 2011;108:14608-14613.

8. Yechoor VK, Patti ME, Ueki K, Laustsen PG, Saccone R, Rauniyar R, Kahn CR. Distinct pathways of insulin-regulated versus diabetes-regulated gene expression: An in vivo analysis in mirko mice. Proc Natl Acad Sci U S A 2004;101:16525-16530.

9. Wagatsuma A, Kotake N, Mabuchi K, Yamada S. Expression of nuclear-encoded genes involved in mitochondrial biogenesis and dynamics in experimentally denervated muscle. J Physiol Biochem 2011;67:359-370.

10. Holmstrom MH, Iglesias-Gutierrez E, Zierath JR, Garcia-Roves PM. Tissue-specific control of mitochondrial respiration in obesity-related insulin resistance and diabetes. Am J Physiol Endocrinol Metab 2012;302:E731-739.

Supplemental Materials and Methods

Ethics Approval and Tissue Handling

The human and animal studies were approved by the appropriate local institutional ethics board for the McGill University Health Centre (BMB 06-018) and the University of Montpellier 1 (NCT00786526) in accordance with World Medical Association guidelines. All human subjects or their surrogates provided written informed consent to participate in the study. Between January and November of 2007, diaphragm and biceps muscle specimens were removed from brain-dead organ donors who had undergone mechanical ventilation (MV group, n=11) for variable periods of time (15-176 hrs); the biopsies were obtained in the operating room prior to circulatory arrest and organ harvest. Sepsis was specifically excluded by clinical criteria and microbial cultures as part of the pre-organ harvest protocol at our institution, and none of the patients received neuromuscular blocking agents in the ICU. Controls consisted of diaphragm samples obtained from age-matched patients during thoracic surgery for benign or malignant lung nodules (n=15), and biceps biopsies from individuals with muscle complaints who were subsequently declared to be normal (n=7). The biceps was employed in MV patients as an internal control to account for any medication or other non-specific effects of critical illness (i.e., those not directly related to mechanical ventilation per se) upon skeletal muscle properties. The biceps was selected because of its similarity to the diaphragm in mixed slow versus fast fiber type composition (1) and its non-weightbearing function. The samples used for biochemical analyses were snap frozen in liquid nitrogen, and those destined for histology were frozen in liquid nitrogen-cooled isopentane. Some analyses could not be performed for all subjects due to small biopsy sample sizes. Biopsy specimens were stored at -80 degrees Celsius, and all of the MV and control group assays were performed concurrently at the McGill University laboratories.

Mitochondrial Enzymatic Activity Assays

Enzymatic activity levels of the mitochondrial oxidative enzymes succinate dehydrogenase (SDH, complex II), cytochrome c oxidase (COX, complex IV) and citrate synthase (CS) were determined spectrophotometrically on muscle homogenates using previously described methods (2). The activity levels of these enzymes are highly correlated with tissue oxidative capacity (3). Muscle samples were kept at -80°C until the day on which experiments were performed. Samples were trimmed of fat and connective tissue and rapidly weighed. Five to 15mg samples were then placed in an ice-cooled petri dish to be finely minced with small scissors before being transferred to a 2ml ice-cooled Potter-Elvehjem glass tissue grinder. A

motorized PTFE teflon pestle was used to homogenize all muscle samples in 50x weight:volume of ice cold extraction buffer containing 200mM Tris, 50 mM triethanolomine and 1 mM EDTA at pH 7.4. Three rounds of 5 cycles of motorized homogenization were applied to each sample, with 10 seconds of rest in between rounds – all procedures were performed on ice. Samples were left on ice until use for biochemical assays. They were then vortexed and diluted 1:20 (10μl in 190μl) in a 96-well plate with the respective assay mix for SDH, COX and CS assays. The average coefficient of variability (C.V.) for enzymatic assays was 13.5%. Protein concentration of each sample was determined using a Bradford protein assay, with an average C.V. of 3.8%. Enzymatic activities expressed either per mg of proteins or per mg of wet muscle weight yielded similar results. All homogenates were prepared on the same day by the same two experimenters.

SDH activity was measured by detecting the decrease in absorbance at 600 nm in a 96-well plate at 30°C, using 200 μl of a reaction buffer (100mM potassium phosphate, 2mM EDTA at pH 7.8) containing (in μM): 100 2,6-dichloroindophenol (DCIP), BSA 1mg/ml, 240 KCN, 4 rotenone, 0.4 antimycin A, 100 decylubiquinone, 200 ATP, and 10mM succinate). COX activity was measured by detecting the decrease in absorbance at 550 nm in a 96-well plate at 30°C, using 200 μl of a reaction buffer (100mM potassium phosphate at pH 7.0) containing 0.1 mM purified reduced cytochrome c and 0.1% n-dodecylmaltoside. CS activity was measured by detecting the increase in absorbance at 412 nm in a 96-well plate at 30°C, using a reaction buffer containing (in μM): 2 acetyl-CoA, 200 5,5'-dithiobis-(2-nitrobenzoic acid) (DTNB), 350 oxaloacetic acid, 0.1% Triton-x). The molar extinction coefficients used were 16.3 L x mol^{-1} x cm^{-1} for DCIP, 13.6 L x mol^{-1} x cm^{-1} for DTNB and 29.5 L x mol^{-1} x cm^{-1} for reduced cytochrome c.

RNA Extraction and Real-time Quantitative PCR (qPCR) for mRNA Levels

Total RNA was extracted from human diaphragm or biceps specimens using TRIZOL reagent (Invitrogen). The isolated RNA was treated with DNase I, followed by further purification using the RNeasy mini kit (Qiagen) according to the manufacturer's instructions. Quantification and purity of total RNA was assessed by A260/A280 absorption. A total of 1 μg of RNA was reverse transcribed using 200 Superscript II Reverse Transcriptase (Invitrogen) in a reaction mixture containing 0.5 m*M* dATP, dCTP, dGTP, and dTTP, 40 units of RNase inhibitor, 50 p*M* random primers and 20 m*M* DTT in a total volume of 20 μl. Real-time PCR was performed by using a *StepOne Plus* Real-Time PCR System (Applied Biosystems). Specific primers were designed to detect the expression of human genes, and Supplemental Table S3 shows all primer sequences. Five microliters of 1:50 diluted reverse-transcriptase reaction was added to 10 μl of RT² SYBR® Green qPCR Master Mixes (Qiagen) and 1 μl of each 10 μ*M* primer. PCR amplification was

carried out for 40 cycles at a melting temperature of 95°C for 15 sec and an annealing temperature of 60°C for 60 sec. A dissociation curve was analyzed for each PCR experiment to assess primer-dimer formation or contamination. Human β-actin was selected as the housekeeping gene from five commonly used housekeeping genes due to its stable expression in comparisons between the MV and control groups. Relative mRNA level quantifications of target genes were determined using the cycle threshold method, and the data were expressed as fold-change compared with the control group.

Gene Expression Profiling

Unsupervised hierarchical clustering analysis (Ward algorithm and complete clustering distance function) was performed and a heatmap was generated using R software (version 2.12.1), including all genes measured that significantly differed ($p < 0.05$) between control and MV diaphragms. Values were log-transformed and the z-score for each value was computed from the mean of each gene. Results of the clustering analyses is displayed as the dendrogram atop the heatmap in Fig. 3F, where shorter "branches" represent a high-degree of similarity in gene expression, and longer branches represent dissimilar expression profiles.

Lipid Staining and Quantification

Eight micron-thick muscle cryosections cut using a cryostat (at -20°C) and mounted to glass slides were used for all histological procedures. For staining of lipids, muscle sections were incubated for 30 minutes with 1% Oil-red-O in 85% propylene glycol. Total lipid content per muscle volume (Fig. 3) was determined by using a protocol adapted from previously described methods (4, 5). Muscle sections were stained with Oil-red-O for 30 minutes, then rinsed three times with tap water. Sections were then individually removed from the glass slides with a razor blade and placed in an 1.5ml Eppendorf tube. Lipids were then eluted with 110µl of isopropanol to release the Oil-red-O dye, which was quantified spectrophotometrically by measuring the absorbance at 450nm of 100µl of the eluded isopropanol at 450nm. A standard curve with pre-determined amounts of Oil-red-O dye was used to determine the amount of dye retained by each section, and results were normalized by the surface area (μm^2) of each section measured microscopically on tiled images prior to removal for elution.

Abundance of intramyocellular lipid (IMCL) droplets (Fig. S1) was quantified by tracing individual fibers using an Intuos5™ Tracing Pad and Image J (version 1.42q, NIH, USA) to determine optical density of approximately 200 individual fibers per subject on binary images. To analyze lipid droplet morphology, we took advantage of the fact that Oil-red-O has

autofluorescent properties (6). Oil-red-O-stained sections were imaged on a confocal Zeiss LSM 3 microscope (excitation = 514nm, emission = 636-657nm in lambda mode), using a PlanApo N 63x/1.40 oil immersion objective and 1.0 digital zoom (pixel size in x,y = 0.07μm, in z = 0.3μm; PMT settings: detection gain=900, offset=0, detector gain=2.5). Imaris 7.0 software was used to analyze z-stacks and produce surface renderings and volume measurements for individual lipid droplets, as shown in Supplemental Fig. S1. Software settings were as follows: smooth 0.1μm, diameter of largest sphere of 1.0μm, threshold for background subtraction of 65-340μm^2, split touching objects enabled, estimated diameter of 0.7μm, quality threshold above 50-140.

Detection of COX Deficient Fibers and Co-localization with Lipid Droplets

For detection of COX deficient fibers or segments, eight-micron thick muscle cryosections were sequentially incubated with 3,3- diaminobenzidine tetrahydrochloride (DAB) + cytochrome c (90 min), followed by nitroblue tetrazolium (NBT) + sodium succinate (90 min) at 37°C to detect the presence or absence of enzymatic activity histologically (*in situ*). Muscle sections from all groups were processed by the same experimenter and stained simultaneously within the same bath. This combined staining technique permits identification of muscle fibers in which COX activity is absent, as previously described in patients with acquired mtDNA deletions (7). Quantification of COX deficient fibers was achieved by digitization of all DAB/NBT-stained slides using a ScanScope XT; fibers from all MV sections were then manually counted by two independent observers and averaged. A total of 88,397 fibers (in cross-section) were counted from transverse sections of MV diaphragms and biceps samples, and fibers were judged COX deficient if blue staining was noticeable in the cytoplasmic area of a fiber. Complete COX deficiency was noticeable by the pure blue color of fibers, whereas partial COX deficiency resulted in grayish fibers. None of the muscle fibers from control subjects presented evidence of COX deficiency by this method. Co-localization of COX deficient segments with lipid accumulation was determined by sequentially staining for COX/SDH activity (as described above) and lipid droplets (Oil-red-O, 45 minutes); sections were then imaged using a Zeiss Axioskop wide field microscope using epifluorescence to detect Oil-red-O staining (8).

Laser Capture Microdissection and Mitochondrial DNA Analyses

Using the same tissue blocks preserved at -80°C used for other histological analyses, 20μm-thick MV diaphragms muscle sections were cut using a cryostat at -20°C. Sections were then mounted on membrane slides (PEN-Membrane 2μm, Leica, catalog no. 11505158) and stained with SDH only to prevent interference of DAB with mtDNA analysis. Serial 10μm-thick dual-

labeled COX-SDH sections were mounted on glass slides and used to identify COX+ and COX deficient cells. Sections were then stored in an air-tight container at -20°C until use. Sections were thawed and allowed to air dry for one hour. We then dissected single muscle cells with a laser capture microdissection microscope (Leica AS LMD 6000), collected in 200µl PCR tubes, lysed individually overnight (10 hours at 55°C, followed by 10 minutes at 95°C) in 15µl of lysis buffer containing Tween-20 (0.67%), Tris HCl (67mM) and proteinase K (0.27µg/µl) at pH 8.5. Lysates were used for real-time PCR multiplex ND1/ND4 assay (9) the following day. Real-time PCR cycling conditions consisted of an initial stage at 50°C for 2 min and 95°C for 10 minutes, followed by 40 cycles of 95°C for 15 sec and 60°C for 1 min. Controls consisted of genomic DNA samples validated by Southern blot for deletion levels, and control real-time PCR amplification curves are shown in Supplemental Fig. S4. We performed long-range PCR (LR-PCR) using Hot Start Takara LA (Takara Biotechnology, Japan) (10) on single cell lysates, and on muscle homogenates which comprised one to four lysed 8µm-thick cyosections. LR-PCR products were resolved using ethidium bromide-loaded agarose (1%) gel electrophoresis for 2 hours. The complete list of primers and probes used for real-time PCR and LR-PCR is provided in Supplemental Table S4.

Western Blot Analyses

Muscle lysates were centrifuged at 13-15,000*g* at 4°C and the resulting supernatants were mixed with sample buffer and boiled for 5 min prior to gel loading. The dilutions of primary and second antibodies were made as per the manufacturers' instructions. The quantification of specific protein bands was performed using the Odyssey® Infrared Imaging System (LI-COR® Biosciences, Lincoln, NE), using either actin or tubulin as a loading control. Antibodies to detect phospho-AMPKα (Thr172) (#2535) and total AMPKα (#2603) were purchased from Cell Signalling Technology, whereas actin (#A3853) and tubulin (#T8328) antibodies were obtained from Sigma.

PRX-3 Transgenic Mice

PRX-3 transgenic mice were a gift from Asubio Pharma (Paramus, NJ) and their generation, as well as the mitochondria-specific localization of the PRX-3 protein in these mice, was previously described in detail (11). In brief, the rat PRX-3 cDNA fragment including the entire open reading frame from nucleotide 5 to 802 was used to create an expression cassette driven by the cytomegalovirus promoter. The genotype was confirmed in each animal by tail clipping and a PCR-based protocol.

Mechanical Ventilation in Mice

Experiments were performed in 8-10 week old male wild-type mice (C57BL/6J) and in homozygous transgenic mice overexpressing PRX-3 on the same background. Non-ventilated mice were acutely euthanized by intraperitoneal (i.p.) injection of pentobarbital sodium (50 mg/kg body weight) without any other previous intervention. We used the same protocol as previously described by our group (12). Briefly, ventilated mice were anesthetized by intraperitoneal injection of pentobarbital sodium (50 mg/kg body weight) and orally intubated with a 22-gauge angiocatheter. No neuromuscular blocking agents were used. General care included continuous maintenance of body temperature using a homeothermic blanket (Homeothermic Blanket Control unit, Harvard Apparatus), and hourly i.p. injections of 0.05ml of Ringer Lactate solution to maintain hemodynamic stability and compensate insensible losses. MV was performed with a small animal ventilator (Minivent®, Harvard Apparatus) using the following ventilator settings: fraction of inspired oxygen of 0.21 (room air), controlled volume mode with tidal volume of 10µl/mg body weight, respiratory rate of 150 breaths/min, and positive end-expiratory pressure (PEEP) level of 3-4 cm H_2O achieved by placing the expiratory port under a water seal. MV parameters and anesthesia were adjusted to prevent spontaneous breathing efforts. The peak airway pressure in MV mice was 11±2 cmH_2O, and the I:E ratio was 1/2. Six hours of MV was employed based upon the fact that this period of MV has been shown to significantly increase oxidative modifications to proteins in the rat diaphragm (13).

Induction of Hyperlipidemia in Mice with P407

Mice were injected intraperitoneally with poloxamer 407 (P407), which is a well established model for inducing hyperlipidemia in mice and rats (14). The mice received a dose of 0.5g per kg of body weight at 24 hours before the initiation of MV. Blood was collected for measurement of serum triglyceride and cholesterol levels when the animals were sacrificed at the end of the MV period.

Measurement of Diaphragm Contractile Properties

Mice were administered pentobarbital to achieve a surgical plane of anesthesia prior to isolating diaphragm strips. After removal, the diaphragm was immediately placed into a chilled (4°C) and equilibrated (95% O_2 - 5% CO_2, pH 7.38) Krebs solution with the following composition (in mM): 118 NaCl, 4.7 KCl, 2.5 $CaCl_2$, 1.2 $MgSO_4$, 1 KH_2PO_4, 25 $NaHCO_3$. A muscle strip ≈2 mm

wide was dissected free, taking care to leave the central tendon and adjacent rib cage margins intact. The excised diaphragm strip was mounted into a jacketed tissue bath chamber filled with equilibrated Krebs solution, using a custom-built muscle holder containing two stimulation electrodes located on either side. A thermoequilibration period of 15 min was observed before initiating contractile measurements at 23°C. After placing the diaphragm strip at optimal length, the force–frequency relationship was determined by sequential supramaximal stimulation using square wave pulses (Model S88; Grass Instruments, West Warwick, RI) for 1 s at 10, 30, 50, 100, and 150 Hz, with 2 min between each stimulation train. The force data were acquired to computer at a sampling rate of 1,000 Hz for later analysis. After completion of the above contractility studies, the muscles were removed from their baths, and muscle length was measured with a microcaliper accurate to 0.1 mm. Muscle force was normalized to tissue cross-sectional area, which was determined by assuming a muscle density of 1.056 g/cm^3. Specific force (force/cross-sectional area) is expressed in Newtons/cm^2.

Measurement of Protein Carbonyls

Protein carbonylation was assessed as an index of oxidative stress, using the Oxyblot Oxidized Protein Detection Kit (Chemicon International). Frozen diaphragm samples were homogenized and prepared for Western blotting according to the manufacturer's instructions, and 10 ug of protein were loaded per well. Optical density measurements of total carbonylated proteins per lane were quantified, normalized to actin protein levels, and expressed as arbitrary units.

Transmission Electron Microscopy

Segments of dissected diaphragm strips measuring 0.2-0.5cm were immediately fixed in 2% gluteraldehyde (Sigma #G5882) in 0.1M cacodylate (Sigma #C4945) buffer, pH 7.4 for a period of two weeks. Samples were post-fixed in 1% osmium tetroxide (Agar Scientific) overnight, and then dehydrated in sequential steps of acetone (25%, 50%, 75% and 100% twice) prior to impregnation in increasing concentrations (25%, 50%, 75% and 100% three times) of resin (TAAB Lab. Equipment) in acetone over a 24-hour period. Samples were then embedded in longitudinal (LS) orientation in 100% resin at 60°C for 24 hours. To verify orientation and section quality, 1µm-thick sections were cut and stained with 1% toluidine blue in 1% borax. Ultrathin sections of 80µm were cut using a diamond knife on an RMC MT-XL ultramicrotome. Sections were stretched with chroloform to eliminate compression and mounted on Pioloform filmed copper grids prior to staining with 2% aquaeus uranyl acetate and lead citrate (Leica). Ultrathin

sections were then examined on a Phillips CM 100 Compustage (FEI) transmission electron microscope and digital images were captured using a AMT CCD camera (Deben). The experimenter was blind to sample identity throughout the procedures. Lipid droplet size was measured by determining the surface area of intermyofibrillar lipid droplets from control and MV animals (n = 3 per group) using Image J (version 1.42q, NIH, USA).

Statistical Analysis

Means ± standard errors (S.E.M.) are presented for all data. Due to the limited amounts of biopsy material, not all of the analyses could be performed in all human subjects (number of subjects for each variable is specifically indicated in figure legends). To account for non-parametric data distribution, all variables were compared between MV and control groups using the Mann Whitney test for unpaired samples. Differences in animal muscle contractility between groups were compared by two-way ANOVA. Unsupervised hierarchical clustering analysis was executed using a Ward algorithm to produce the heatmap (R Foundation for Statistical Computing, version 2.12.1). Results of the clustering analyses is displayed as the dendrogram atop the heatmap in Fig. 2D. Other statistical analyses were performed using PASW 18 (IBM) and Prism 5 (Graphpad).

SUPPLEMENTAL REFERENCES

1. Pereira MC, Isayama RN, Seabra JC, Campos GE, Paschoal IA. Distribution and morphometry of skeletal muscle fibers in patients with chronic obstructive pulmonary disease and chronic hypoxemia. *Muscle Nerve* 2004;30:796-798.

2. Picard M, Ritchie D, Wright KJ, Romestaing C, Melissa MT, Rowan SL, Taivassalo T, Hepple RT. Mitochondrial functional impairment with aging is exaggerated in isolated mitochondria compared to permeabilized myofibers. *Aging Cell* 2010;9:1032-1046.

3. Schwerzmann K, Hoppeler H, Kayar SR, Weibel ER. Oxidative capacity of muscle and mitochondria: Correlation of physiological, biochemical, and morphometric characteristics. *Proc Natl Acad Sci U S A* 1989;86:1583-1587.

4. Sen A, Lea-Currie YR, Sujkowska D, Franklin DM, Wilkison WO, Halvorsen YD, Gimble JM. Adipogenic potential of human adipose derived stromal cells from multiple donors is heterogeneous. *J Cell Biochem* 2001;81:312-319.

5. Salehzada T, Cambier L, Vu Thi N, Manchon L, Regnier L, Bisbal C. Endoribonuclease l (rnase l) regulates the myogenic and adipogenic potential of myogenic cells. *PLoS One* 2009;4:e7563.

6. Shaw CS, Jones DA, Wagenmakers AJ. Network distribution of mitochondria and lipid droplets in human muscle fibres. *Histochem Cell Biol* 2008;129:65-72.

7. Taylor RW, Turnbull DM. Mitochondrial DNA mutations in human disease. *Nat Rev Genet* 2005;6:389-402.

8. Koopman R, Schaart G, Hesselink MK. Optimisation of oil red o staining permits combination with immunofluorescence and automated quantification of lipids. *Histochem Cell Biol* 2001;116:63-68.

9. Krishnan KJ, Bender A, Taylor RW, Turnbull DM. A multiplex real-time pcr method to detect and quantify mitochondrial DNA deletions in individual cells. *Anal Biochem* 2007;370:127-129.

10. Bender A, Krishnan KJ, Morris CM, Taylor GA, Reeve AK, Perry RH, Jaros E, Hersheson JS, Betts J, Klopstock T, et al. High levels of mitochondrial DNA deletions in substantia nigra neurons in aging and parkinson disease. *Nat Genet* 2006;38:515-517.

11. Matsushima S, Ide T, Yamato M, Matsusaka H, Hattori F, Ikeuchi M, Kubota T, Sunagawa K, Hasegawa Y, Kurihara T, et al. Overexpression of mitochondrial peroxiredoxin-3 prevents left ventricular remodeling and failure after myocardial infarction in mice. *Circulation* 2006;113:1779-1786.

12. Jung B, Mrozek S, Petrof B, Lacampagne A, Matecki S, Jaber S. Ventilator-induced diaphragmatic dysfunction: Development and perspectives of the first mouse model. *Am J Respir Crit Care Med* 2011;183:A4245.

13. Zergeroglu MA, McKenzie MJ, Shanely RA, Van Gammeren D, DeRuisseau KC, Powers SK. Mechanical ventilation-induced oxidative stress in the diaphragm. *J Appl Physiol* 2003;95:1116-1124.

14. Johnston TP. The p-407–induced murine model of dose-controlled hyperlipidemia and atherosclerosis: A review of findings to date. *J Cardiovasc Pharmacol* 2004;43:595-606.